2020 년 8 월

박사학위 논문

Functional study of REDD1 as a novel therapeutic target for the ferroptosis-mediated liver fibrosis

조선대학교 대학원

약 학 과

조 삼 석

Functional study of REDD1 as a novel therapeutic target for the ferroptosis-mediated liver fibrosis

페롭토시스 매개 간섬유화의 신규 치료표적으로써
REDD1 의 기능 연구

2020 년 8 월 28 일

조선대학교 대학원

약 학 과

조 삼 석

Functional study of REDD1 as a novel therapeutic target for the ferroptosis-mediated liver fibrosis

지도교수 기 성 환

이 논문을 약학 박사학위신청 논문으로 제출함

2020 년 5 월

조선대학교 대학원

약 학 과

조 삼 석

조삼석의 박사학위논문을 인준함

위원장 조선대학교 교수 최 홍 석 인

위 원 동신대학교 교수 양 지 혜 인

위 원 전남대학교 교수 조 영 창 인

위 원 조선대학교 교수 이 금 화 인

위 원 조선대학교 교수 기 성 환 인

2020 년 7 월

조선대학교 대학원

CONTENTS

LIST OF FIGURES

Part I: The effect of ferroptosis in hepatic stellate cell activation

Part II: The role of REDD1 in liver fibrosis

ABBREVIATIONS

α-SMA	Alpha-smooth muscle actin
ActD	Actinomycin-D
Ad-LacZ	Adenovirus expressing LacZ
Ad-REDD1	Adenovirus expressing REDD1
ALT	Alanine aminotransferase
AMPK	Adenosine monophosphate-activated protein kinase
AP-1	Activator protein 1
AST	Aspartate aminotransferase
CCl_4	Carbon tetrachloride
CQ	Chloroquine
DCFH-DA	2′,7′-Dichlorofluorescein diacetate
DFO	Deferoxamine
DN-AMPK	Dominant-negative mutant form of AMPK
ECM	Extracellular matrix
ERK	Extracellular signal-regulated kinase
Fe-NTA	Ferric nitrilotriacetate
Fer-1	Ferrotstatin-1
GPX1	Glutathione peroxidase 1
GPX4	Glutathione peroxidase 4

GSH	Glutathione
H&E	Hematoxylin and eosin
HSCs	Hepatic stellate cells
JNK	c-JUN N-terminal kinase
MAPK	Mitogen-activated protein kinase
MDA	Malondialdehyde
mTOR	Mammalian target of rapamycin
MTT	3-(4,5-Dimethylthiazol-2-yl)-2,5-diphenyl-tetrazolium bromide
Nec-1	Necrostatin-1
PHZ	Phenylhydrazine
PAI-1	Plasminogen activator inhibitor-1
PCR	Polymerase chain reaction
REDD1	Regulated in development and DNA damage response 1
ROS	Reactive oxygen species
SBE	Smad-binding element
SE	Standard error
TfR-1	Transferrin receptor-1
TGF-β	Transforming growth factor-β

국 문 초 록

페롭토시스 매개 간섬유화의 신규 치료표적으로써 REDD1 의 기능 연구

조 삼 석

지 도 교 수: 기 성 환

약학과

조선대학교 대학원

페롭토시스(Ferroptosis)는 세포 내 글루타티온 고갈과 철분 축적에 따른 펜톤산화에 의해 지질과산화물이 축적되어 세포장애를 유발하는 세포사멸의 한 종류로 세포자연사(apoptosis)와는 구별된다. 간섬유화는 알코올, 간염바이러스, 독성물질 등의 다양한 원인에 의한 반복적인 간 손상으로 세포 외 기질(extra cellular matrix)이 축적되어 발생한다. 세포 외 기질의 축적은 간섬유화의 주요 원인이며, 간성상세포에서 주로 생성된다. 간성상세포는 평상 시 휴지기(quiescent)상태로 유지되지만, 만성적인 간 손상 시 활성화(activation)되어 세포 외 기질 생산 및 분비를 증가시켜 간섬유화 진행에 핵심적인 역할을 한다. 최근 페롭토시스는 아세트아미노펜에 의한 급성간부전, 비알콜성지방간염의 진행을 매개하고, 간암세포에서 세포독성 유발로 인해 항암요법의 새로운 표적으로 보고 된 바 있다. 이처럼 다

양한 간질환들과 페롭토시스의 연관성을 규명하는 연구가 활발히 진행되고 있으나, 간섬유화에서 페롭토시스에 대한 연구는 부족한 실정이다.

REDD1 은 활성산소종과 DNA 손상, 저 산소 상태 등의 다양한 스트레스 상황에 반응하여 세포생존에 관여하는 단백질로 알려져 있다. REDD1 의 발현 및 활성화 조절을 매개하는 주요 조절인자로는 p53, HIF-1α, AP-1 등이 있으며, 이들은 스트레스에 의해 매개되어 활성화되는 전사인자로 잘 알려져 있다. 또한, 이전에 간세포에서 산화적스트레스에 의한 손상에 대하여 REDD1 유전자의 보호효능에 관해 보고 한 바 있다. 그러나, 간섬유화 진행 시 활성화되는 간성상세포에서 REDD1 의 조절 기전 및 역할에 대한 연구는 전무하다. 따라서, 본 연구에서는 간성상세포의 활성화에 있어서 페롭토시스의 기능적 역할, 더 나아가 간섬유화 진행 시 치료표적으로써 REDD1 의 가능성을 탐색하고자 하였다.

첫 번째로, 본 연구에서는 간성상세포에서 페롭토시스 유도제에 의한 세포사멸이 세포자연사(apoptosis) 및 세포자멸괴사(necroptosis)와 구별되며 페롭토시스 특이적 표지자들의 변화를 통해 페롭토시스의 발생을 관찰하였다. 또한, 페롭토시스가 Smad 비의존적인 경로인 AP-1 신호전달 경로를 통해 간성상세포의 활성화에 기여함을 확인하였다. 더 나아가 마우스에 만성적으로 과량의 철을 투여한 경우, 간 섬유화의 발생이 인정되었다. 이는, 간성상세포에서 페롭토시스의 발생이 간섬유화 발병에 기여할 수 있음을 시사한다.

두 번째로, 만성 간질환 모델인 간섬유화 모델에서 스트레스 반응유전자인 REDD1 의 역할을 규명하였다. 먼저, 본 연구자들이 확립한 과량의 철분투여에 따른 간섬유화 동물모델에서 REDD1 유전자의 하향조절이 관찰되었다. 이는 만성질

환으로 이행에 따른 REDD1 유전자의 보호 효능 소실 때문 인 것으로 보인다. 반면, 간성상세포주인 LX-2 세포에서 섬유성 사이토카인인 TGF-β에 의한 REDD1 유전자의 상향조절이 관찰되었는데, 이는 REDD1 유전자가 초기 스트레스반응에 유도되어 보호 효능을 나타내는 것으로 보인다. 또한, TGF-β에 의한 REDD1 유전자의 발현은 AP-1 을 경유하는 전사적인 조절임을 확인하였다. LX-2 세포에서 TGF-β에 의해 유도되는 섬유화 지표들(α-SMA, PAI-1)이 REDD1 유전자 과발현에 의해 현저히 억제되는 것이 관찰되었다. 사염화탄소(CCl_4) 투여에 의한 간섬유화 동물모델에서도 아데노바이러스를 이용한 REDD1 유전자 과발현에 의해 ALT, AST 수치 및 간 섬유화지표들의 현저한 억제가 관찰되었다.

결과적으로, 본 연구에서는 간섬유화 발병에 대한 페롭토시스의 기능적 역할을 간성상세포를 중심으로 규명하고, REDD1 의 조절기전 및 항섬유화 효능을 규명하여 페롭토시스 매개 간섬유화의 치료표적으로써 REDD1 의 가능성을 제시하였다.

I. INTRODUCTION

Ferroptosis and liver disease

Ferroptosis is an oxidative, iron-dependent nonapoptotic, peroxidation-driven form of regulated cell death that is morphologically, biochemically, and genetically distinct from apoptosis, necrosis, autophagy, and other types of cell death (Yagoda et al. 2007, Yang and Stockwell 2008, Dixon et al. 2012, Fatokun et al. 2014). While apoptosis is mediated by pro-death molecules such as BCL2-associated X protein, ferroptosis is initiated by GSH depletion or GPX4 inactivation (Dixon et al. 2012, Yang et al. 2014). Poly (ADP ribose) polymerase 1 cleavage, release of cytochrome c from mitochondria, or cleavage of pro-caspase-3 were not also observed during ferroptosis (Yagoda et al. 2007, Yang et al. 2014). Moreover, there are distinguishable characters of mitochondrial morphology during ferroptosis, smaller than normal mitochondria with condensed mitochondrial membrane densities, reduced or absent mitochondria crista and outer mitochondrial membrane rupture (Yagoda et al. 2007, Dixon et al. 2012, Xie et al. 2016). In addition, ferroptosis is characterized by an iron-mediated excessive peroxidation of polyunsaturated fatty acid (PUFA)-containing phospholipids, exist in mammalian cell membranes (Dixon et al. 2015). Treatment of iron chelators (deferoxamine) or antioxidants (vitamine E, ferrostatin-1, or liproxstatin-1) can reverse the lipid peroxidation of ferroptosis (Dixon et al. 2012, Friedmann Angeli et al. 2014). Although ferroptosis is considered as an essential mechanism for sustaining cell survival, rendering some cells extremely susceptible to ferroptotic cell death. Recently, ferroptosis has gained lots of interest, especially in view of the modulation of genes involved in ferroptosis or introduction of ferroptosis-inducing agents in liver diseases, such as hepatocellular carcinoma (HCC), liver fibrosis, liver failure and alcoholic/nonalcoholic fatty liver diseases.

1. The Mechanism of Ferroptosis

Dr. Brent R. Stockwell *et al*. used the 'ferroptosis' to explain cell death caused by the accumulation of iron-dependent lipid peroxide in 2012. Ferroptosis is induced by inactivating glutathione peroxidase 4 (GPX4), a major protective mechanism of membranes against peroxidation damage (Bochkov et al. 2010, Dixon et al. 2012, Dixon and Stockwell 2014). Loss of GPX4 activity is mediated by direct or indirect mechanism such as depletion of glutathione (GSH), acting as a crucial cofactor of GPX4 (Dixon et al. 2012, Yang et al. 2014).

Ferroptosis Induction by Inhibition of System X_c^-

System X_c^- is a Na^+-dependent cysteine-glutamate exchange transporter, which is a disulfide-linked heterodimer consisted of a heavy-chain subunit (CD98hc, SLC3A2) and a light-chain subunit (xCT, SLC7A11) (Sato et al. 1999). While it transfers intracellular glutamate to the extracellular space, system X_c^- transports extracellular cysteine into the cell, which is then changed into cysteine for GSH synthesis. By utilizing GSH as a cofactor, GPX4 acts as a crucial cellular antioxidant defenses against phospholipid peroxides. Hence, the inhibition of system X_c^- induces GSH depletion and sequentially indirectly inactivates GPX4, leading to accumulation of toxic lipid ROS and the initiation of ferropotosis (Dixon et al. 2012, Yang et al. 2014). Direct suppression of GSH synthesis via inhibition of glutamate-cysteine ligase (e.g. buthionine sulfoximine) can cause ferroptosis (Yang et al. 2014).

Ferroptosis Induction by Direct inhibition of GPX4

GPX4 was originally considered a lipid peroxidation suppressor since it degrades H_2O_2 and organic H_2O_2 into water or alcohols, and uses GSH as an essential cofactor to activate (Brigelius-Flohe and Maiorino 2013). (1S, 3R)-RSL (RSL3) is a classical ferroptosis inducer that can

directly bind to GPX4 and inhibit its activity by covalently targeting selenocysteine in an irreversible manner, leading to the intracellular accumulation of lipid peroxides and subsequent ferroptosis (Yang et al. 2014, Yang et al. 2016). In addition to erastin and RSL3, other 12 ferroptosis inducers have been discovered in a large number of screening experiments (Weiwer et al. 2012, Yang et al. 2012). Eight of these inducers (DPI7, DPI10, DPI12, DPI13, DPI17, DPI18, DPI19, and RSL3) can directly suppress GPX4 activity. FIN56, a new and specific ferroptosis inducer, mediates decrease of GPX4 abundance (Shimada et al. 2016). Consistently, GPX4 deletion generates the rapid accumulation of lipid ROS and induces ferroptotic cell death (Yang et al. 2012, Friedmann Angeli et al. 2014). Ectopic expression of GPX4 facilitates cell viability induced by these compounds, but not by other cytotoxic agents, implying that GPX4 is currently believed to be a specific and robust central controller of ferroptosis (Yang et al. 2012).

2. The Modulator of Ferroptosis

Considering the fact that the initiation of ferroptosis is closely related to iron, ROS, and PUFAs, a variety of genes and signaling pathways related to metabolism in iron, lipid synthesis, and oxidative stress have been identified, which potentially modulate the vulnerability to ferroptosis (Hassannia et al. 2019).

Iron metabolism

It is notable that iron plays an essential role in execution of ferroptosis (Dixon and Stockwell 2014). Iron is an important component for most organisms of cellular processes, such as oxygen transport, mitochondrial respiration, DNA replication, and cell signaling. Although it exists abundantly in the environment, its bioavailability is limited since iron ions present as ferric (Fe^{3+}) form, which is insoluble in aqueous solutions at physiological pH. Iron ions can exist both in the

ferric and the ferrous (Fe^{2+}) forms, allowing them to function as the transition metal to easily donate or accept electrons to participate in oxidation-reduction reactions (Andrews and Schmidt 2007, Verbon et al. 2017). However, excess free Fe^{2+} iron (LIP) is present inside a cell leads to the formation of hydroxyl radicals via the Fenton reaction, which can lead cytotoxicity caused by damages of DNA, protein, and lipids (Luo et al. 1994). Normally, the intracellular iron maintains a delicate regulatory system. Extracellular iron can be imported by transferrin (TF) and its carrier protein transferrin receptor (TFR). Imported iron is stored and transported as the form of ferritin. Intracellular iron can be exported by ferroportin (FPN) (Hentze et al. 2010). Increasing LIP by either increased iron import or reduced iron export can increase sensitivity to oxidative damage and ferroptosis.

Besides the amount of LIPs in cells, other genes related to iron metabolism also affect ferrroptosis. Nuclear receptor coactivator 4 (NCOA4) is a cargo receptor mediating the transport of ferritin to autophagosomes for lysosome-dependent degradation and iron release (i.e. ferritinophagy), which can accumulate large amounts of iron, and NCOA4 inhibition leads to attenuation of ferroptosis (Hou et al. 2016). Iron-response element binding protein 2 (IREB2) encodes the master regulator of iron metabolism including TF, TFR1, ferritin (Dixon et al. 2012, Bogdan et al. 2016). Silencing of IREB2 significantly suppressed erastin-induced ferroptosis. Excessively increased activity of HMOX1, a mediator of the degradation of heme to ferrous iron, biliverdin and carbon monoxide, induces increased of LIP and subsequently initiate ferroptosis (Chang et al. 2018, Hassannia et al. 2019). However, a moderate upregulation of HMOX1 can protect cells based on its anti-oxidant activity (Suttner and Dennery 1999).

ROS metabolism

ROS, considered as one of the most important indicators of ferroptosis, is a partially reduced

oxygen molecule including peroxides (H2O2), superoxide (O2-·), singlet oxygen (1O2), and free radicals (HO·, RO·, NO·, and NO2·) generated from various sources. GSH is a pivotal factor for ferroptosis by maintaining the cellular oxidation-reduction balance. GSH mediates the reduction of the toxic phospholipid hydroperoxides into nontoxic phospholipid alcohols via GPX4. Hence, this character enables GPX4 to play a central downstream regulator of ferroptosis (Yang et al. 2014). In presence of ROS, cystathionine-β-synthetase activation promotes methionine-to-cysteine conversion and GSH synthesis through the transsulfuration pathways, thus protecting cells from the injury caused by ROS (McBean 2012). Recent research shown that increase of the transsulfuration related genes in response to the loss of certain tRNA synthases could inhibit erastin-induced ferroptosis (Hayano et al. 2016).

Lipid metabolism

The mevalonate pathway regulates sensitivity to ferroptosis. A direct metabolite of mevalonate, isopentenyl-pyrophosphate (Distefano et al.) is important product for cholesterol synthesis, isopentenylation of selenocysteine tRNA and CoQ10 production (Moosmann and Behl 2004). Repressing the activity of squalene synthase or squalene monooxygenase, which are downstream of isopentenyl-pyrophosphate involved in cholesterol synthesis, impedes ferroptosis. Statin-mediated inhibition of HMG-CoA reductase, upstream of isopentenyl-pyrophosphate synthesis, promotes ferroptosis (Shimada et al. 2016). Additionally, mevalonate pathway also affects ferroptosis by regulating the synthesis of selenoprotein, which exists in the active center of GPX4 with selenocysteine. Suppressing of isopentenyl-pyrophosphate production interferes maturation of selenocysteine tRNA, a specific transporter for the incorporation of selenocysteine into GPX4. Moreover, suppression of coenzyme Q10 synthesis can induce mitochondrial damage which enhances ferroptosis.

The Inducers of Ferroptosis

There are various types of substances that induce ferroptosis, such as erastin, RSL3, sorafenib and FIN56. Most of ferroptosis inducers were actually discovered before the notion of ferroptosis was identified. Firstly, erastin has been identified as a new synthetic compound that induce RAS-mutated tumor cells death in the absence of apoptosis (Dolma et al. 2003). Ras-selective lethal small molecule (RSL)-3 was later identified as a compound with similar effects to erastin (Yang and Stockwell 2008). After the ferroptosis was established (Dixon et al. 2012), it was confirmed that other compounds such as sorafenib and FINO2 induced ferroptosis. Recently, these substances are classified into several types according to mechanism underlying ferroptosis induction.

First, class I ferroptosis inducers, such as erastin and sorafenib, deplete cysteine in cells by inhibiting system Xc^-. Cysteine depletion in the cells inhibit biosynthesis of GSH, which results in loss of GPX4 activity. Eventually, ferroptosis is caused by the accumulation of lipid peroxidation.

Class II ferroptosis inducers including RSL3 and DPI compounds (7, 10, 12, 13, 17, 18, 19) act by directly inhibiting GPX4. They inhibit the GPX4 activity by covalently interacting with the active site in selenocysteine of GPX4 (Yang et al. 2016), which inactivates GPX4 subsequently leading to lipid peroxidation accumulation and cell death.

Class III ferroptosis inducers act by decreasing GPX4 protein abundance and causing depletes coenzyme Q10 (CoQ10) via squalene synthetase-mevalonate pathway. Coenzyme Q10 is an endogenous cellular antioxidant and well-known as an essential component in mitochondrial electron transport chain (Shimada et al. 2016). FIN56 is a representative compound of Class III ferroptosis inducers.

Class IV ferroptosis inducer act to induces lipid peroxidation and indirectly loss of GPX4

activity. FINO2 is the only compound known to date as a class IV ferroptosis inducer. FINO2 both indirectly inhibits GPX4 activity and bypasses GSH depletion to cause iron oxidation, consequentially causing widely lipid peroxidation (Gaschler et al. 2018).

Table 1. Ferroptosis inducers and its inhibitors

	Reagent	Impact on ferroptosis	Target/Function	References
Inducers				
Class I	Erastin, Piperazine Erastin (PE), Imidazole Ketone Erastin (IKE), Sorafenib	Prevent cysteine import, causes GSH depletion	System Xc^-	(Dixon *et al.*, 2012, Sun *et al.*, 2016, Zhang *et al.*, 2019, Yang *et al.*, 2014)
Class II	RSL3, ML162, DPI compounds 7,10,12,13,17,18,19	Covalent inhibitor of GPX4 that causes accumulation of lipid peroxidation	GPX4	(Yang *et al.*, 2014)
Class III	FIN56 and CIL56	Depletes CoQ10 via SQS-mevalonate pathway and causes decrease in GPX4 protein abundance	Depletion of GPX4 protein and CoQ10	(Shimada *et al.*, 2016)
Class IV	FINO2	Induces lipid peroxidation and loss of GPX4 activity	Induction of lipid peroxidation	(Gaschler *et al.*, 2018)
Inhibitors				
Class I	Deferoxamine mesylate	Suppress accumulation of iron		(Skouta *et al.*, 2014)
Class II	Ferrostatin-1, vitamin E, liproxstatin-1, SRS11-9, SRS16-86	Prevent lipid peroxidation		(Skouta *et al.*, 2014)

3. Ferroptosis in liver diseases

There is accumulative evidence the connection between ferroptosis and the pathogenesis of diverse liver diseases such as hepatocellular carcinoma (HCC), fibrosis, liver failure and nonalcoholic/alcoholic steatohepatitis.

Ferroptosis and HCC

HCC is the most frequent type of primary liver cancer and is the second leading cause of cancer-related mortality worldwide (Knudsen et al. 2014). Despite treatment for advanced HCC including surgical resection and nonsurgical therapies are of limited effectiveness, the

mechanisms underlying development and progression of HCC should be identified further (Llovet et al. 2008). Intriguingly, it has been revealed the versatile ferroptosis inducers exert cytotoxicity on HCC. Depletion of the intracellular iron by using iron chelator deferoxamine strikingly preserve HCC cells against the cytotoxic effects of sorafenib (Louandre et al. 2013). In addition, inhibition of transsulfuration via cystathione β-synthase suppresses HCC cell proliferation and significantly reduces *in vivo* tumor growth. A representative transcription factor for expression antioxidant gene Nrf2 has an inhibitory role of inducing both HCC survival and death. Nrf2 protects HCC against ferroptosis upon exposure to erastin, sorafenib, or buthionine sulfoximine. This was derived from the inhibitory effect of p62 on Nrf2 degradation by Keap1 (Sun et al. 2016). Besides, activation of Nrf2 contributes to sorafenib resistance of HCC by upregulation of metallothionein-1G and sigma-1 receptor (Sun et al. 2016, Bai et al. 2017). Upon exposure to sorafenib, the Rb-deficient HCC cells promote the occurrence of ferroptosis, suggesting that Rb is involved in sorafenib-induced ferroptosis (Louandre et al. 2015). Deletion of ceruloplasmin stimulates erastin- and RSL3-induced ferroptotic cell death and resulted in the accumulation of intracellular Fe^{2+} and lipid ROS (Shang et al. 2020). BRCA1-associated protein 1, a nuclear deubiquitinating enzyme to reduce histone 2A ubiquitination on chromatin, represses SLC7A11 expression leading to elevated lipid peroxidation and ferroptosis (Zhang et al. 2018). Moreover, there is an interesting study revealed that two transcription factors, HIC1 and HNF4A have been identified to differentially and transcriptionally affect ferroptosis-controlling genes; HIC1 facilitates ferroptosis and HNF4A conversly acts to ferroptosis (Zhang et al. 2019). Recently, it is demonstrated that erastin treatment increases ferroptosis via changes of the long non-coding RNA GABPB1-AS1, which downregulates GABPB1 protein levels through blocking GABPB1 translation, eventually decreases the level of peroxiredoxin-5 peroxidase (Qi et al. 2019). Based on these observations, induction of ferroptosis has been suggested as an anti-

cancer therapy target.

Ferroptosis and nonalcoholic steatohepatitis (NASH)

NASH is characterized by lipid accumulation within hepatocytes, death of hepatic cells, infiltration of inflammatory cells, and fibrosis (Liu et al. 2016). Recent studies have revealed that a role for ferroptosis during the progression of NASH. There is a report that hepatic ferroptosis has been shown to act as a trigger at the onset of NASH. Ferroptosis inhibitors, trolox and deferoxamine treatment alleviated cell death, and infiltration of inflammatory cytokine production, and the amount of oxygenated phosphatidylethanolamine, which is implicated that ferroptosis pathway is increased in the liver of choline-deficient, ethionine-supplemented diet-induced steatohepatitis mice model compared with normal diet-fed mice. A study shown that hepatic phosphatidylcholine/phosphatidylethanolamine ratios are decreased in NASH patients consistently support this notion (Tsurusaki et al. 2019). In another study, decreased hepatic expression of GPX4 is observed in mice liver fed methionine/choline-deficient diet (MCD) with RSL-3 treatment, indicating that ferroptosis plays a key role in NASH-related lipid peroxidation and its associated cell death. Conversely, deferoxamine and sodium selenite (a GPX4 activator) significantly reduced NASH severity and abolished the harmful effects of RSL-3 in MCD-fed mice (Qi et al. 2020).

Ferroptosis and acute liver failure (ALF)

ALF is a serious disorder caused by various factors such as liver synthesis, detoxification, excretion and biotransformation. It has been implicated that ferroptosis plays a role in the development of ALF. Ferroptosis mediates acetaminophen-induced hepatotoxicity (Lorincz et al. 2015). Lipid peroxidation leads to hepatocyte ferroptosis, resulting in acute liver failure.

Glycirrhizin reduced the level of ferroptosis during ALF, which may depend on the inhibition of oxidative stress pathway via Nrf2/HO-1/HMGB1 pathway (Wang et al. 2019).

REDD1 is known as stress response gene that induced by various cellular stresses, such as hypoxia, glucocorticoid and DNA damage (Wang et al. 2006, Shoshani, 2002, Ellisen, 2002). Furthermore, it has been reported that REDD1 negatively regulates mammalian target of rapamycin (mTOR) through tuberous sclerosis complex (TSC) 1/2. mTORC1 is well known as regulator of cell survival and proliferation (Molitoris et al. 2011). Besides, it has been reported that REDD1 involved in a variety of roles on cell proliferation, tumor invasion, tumorigenesis (Molitoris et al. 2011, Chang, 2009, Wang, 2003, Ota, 2014). However, there is a controversial role of REDD1 related to ROS. It has been reported that REDD1 forms a stress-inducing complex with TXNIP and increases oxidative stress and cell death (Qiao et al. 2015). On the other hand, it is also reported that REDD1 protects cells from hypoxia by reducing ROS formation (Horak et al. 2010).

Although studies on the association between ferroptosis and liver diseases are being conducted recently, there is no research on ferroptosis in liver fibrosis, which is mediated by HSCs activation. Thus, we currently tried to identify the role of ferroptosis in HSCs and establish cell or animal models of ferroptosis-mediated hepatic fibrosis. Moreover, we demonstrate the role of REDD1 as a novel therapeutic target for the ferroptosis-mediated liver fibrosis.

Ⅱ. MATERIALS AND METHODS

Materials

Caspase-3, phospho-Smad3, Smad2/3, p-cJUN and c-JUN antibodies were provided by Cell Signaling Technology (Danvers, MA). Transferrin receptor 1, GPX4 and ferroportin antibodies were purchase from Abcam (Cambridge, UK). The REDD1 antibody was acquired from Proteintech (Chicago, IL, USA). PARP and Smad7 antibodies were obtained from Santa Cruz Biotechnology (Santa Cruz, CA). C11-BODIPY fluorescent dye, goat anti-rabbit and anti-mouse secondary antibodies were purchased from Invitrogen (Carlsbad, CA, USA). TGF-β1 recombinant protein was supplied from R&D Systems (Minneapolis, MN, USA). Erastin and RSL3 were purchased from Selleck Chemicals (Houston, TX, USA). Mitogen-activated protein kinase (MAPK) inhibitors for ERK (PD98059), p38 (SB203580), and JNK (SP600125) were obtained from Calbiochem (Billerica, MA, USA). 3-(4,5-dimethylthiazol-2-yl)-2,5-diphenyl-tetrazolium bromide (MTT), 2′,7′-dichlorofluorescein diacetate (DCFH-DA), actinomycin-D (ActD), Ferrostatin-1 (Fer-1), Deferoxamine (DFO), ZVAD-FMK, Necrostatin-1 (Nec-1), Iron (Ⅲ) nitrate nonahydrate, Nitrilotriacetic acid disodium salt, Iron dextran and β-actin antibody were purchased from Sigma-Aldrich (St. Louis, MO, USA).

Cell culture

LX-2 cells (human immortalized HSCs) were provided by Dr. S.L.Friedmann (Mount Sinai School of Medicine, New York, NY). HSC-T6 cell line was purchased from ATCC (American Type Culture Collection, Manassas, VA). Cells were grown in Dulbecco's modified Eagle's medium (DMEM) containing 50 units/mL penicillin/streptomycin and 10% fetal bovine serum

(FBS) at 37℃ in a humidified 5% CO_2 atmosphere. Cells were washed twice with ice-cold phosphate buffered saline (PBS) before sample preparation.

Isolation of Hepatic stellate cells (HSCs)

HSCs were isolated from the liver of 8 weeks old male mice (Oriental Bio, Sungnam, South Korea) as previously reported (Jin et al. 2013, Kim et al. 2018). The protocols of all animal experiments were reviewed and approved by the Animal Care and Use Committee of Chosun University. After intubation in the portal vein, the livers were perfused in situ with Ca^{2+}-free Hank's balanced saline solution at 37°C for 20 min and then perfused with solution containing 0.05% collagenase and Ca^{2+} for 20 min, at a flow rate of 10 mL/min. The perfused livers were minced, filtered through 70 μm cell strainer (BD Bioscience), and centrifuged at 50 g for 3 min to separate the hepatocytes. Primary HSCs were isolated by gradient centrifugation, as previously reported (Jin et al. 2013, Kim et al. 2018). Isolated primary HSCs and LX-2 cells were cultured on uncoated dishes. Quiescent HSCs were cultured for 0 day, and activated HSCs were cultured for 7 days.

MTT assay

To measure cytotoxicity, LX-2 cells were plated at 24-well plates and incubated with Erastin or RSL3 for 24 h. After treatment, cells were stained with MTT (0.2 mg/mL and incubated for 1 h). The media were then removed and any formazan crystals produced in the wells were dissolved with the addition of 300 μL of dimethyl sulfoxide (DMSO). Absorbance at 550 nm was measured using microplate reader (SpectraMAX, Molecular Device, Sunnyvale, CA). Cell viability was defined relative to the untreated control [i.e., viability (% control) = 100 × (absorbance of treated sample) / (absorbance of control)].

Immunoblot analysis

Total cell lysates were prepared as previously reported (Yuan et al. 2009). The cells were centrifuged at 3,000 x g for 3 min and allowed to lysis after the addition of lysis buffer (RIPA). Lysates were centrifuged at 12,000 g for 15 min to obtain supernatant. After protein extraction, sodium dodecyl sulfate–polyacrylamide gel electrophoresis, and immunoblotting were carried out, as previously reported (Kim et al. 2015). Signals in nitrocellulose membranes were visualized by using a chemiluminescence detection system (GE Health care, Chalfont St. Giles, United Kingdom).

RNA isolation and quantitative real-time PCR (RT-PCR)

Cells were lysed using Trizol reagent (Invitrogen, USA) and total RNA was extracted with chloroform and isopropanol. To obtain cDNA, total RNA (2 μg) was reverse-transcribed using an oligo dT_{18} primer. The cDNA was amplified using an Accupower RT premix (Bioneer, Daejeon, Korea). Real-time PCR was carried out using a SYBR Green Premix (Applied Biosystems, Foster City, CA) and a Step One Real-time PCR System (Applied Biosystems). The sequences of the primers were as follows: human PAI-1 5'-CGCCAGAGCAGGACGAA-3' (forward) and 5'-CATCTGCATCCTGAAGTTCTCA-3' (reverse); human TIMP-1 5′-GGTGGGTGGATGAGTAATGC-3′ (forward), 5′-CAGCGGCTGCGGAAAC-3′ (reverse); human Glyceraldehyde-3-phosphate dehydrogenase (GAPDH) 5′-GAAGGTGAAGGTCGGAGTC-3′ (forward), 5′-GAAGATGGTGATGGGATTTC-3′ (reverse); human REDD1 5′-GAGCCTGGAGAGCTCGGACT-3′ (forward) and 5′-CTGCATCAGGTTGGCACACA-3′ (reverse). GAPDH was used as an internal control and relative levels of specific gene were determined by $2^{-\Delta\Delta CT}$ method. As another method of

obtaining results, amplified products were resolved by using 2% agarose gel, stained with ethidium bromide, and visualized by a transilluminator.

Construction of plasmids, transient transfection and reporter gene assay

Luciferase reporter plasmid, phREDD1–2548 and pCMV6-AC-GFP-REDD1 plasmid were provided by Dr. Xiao (Armed Forces Radiobiology Research Institute, Bethesda, MD, USA). The pCDNA3-Flag-Smad3 and SBE-Luc [pGL3-(CAGA)9-MLP-luciferase] were kindly provided by Prof. H.S. Choi (Chonnam National University, Gwangju, Korea) (Cho et al. 2010). Serial deletion mutants of human REDD1 promoter and deletion mutant of putative AP-1 binding site were constructed, as previously reported (Cho et al. 2018). LX-2 cells in 12-well plates were serum starved for 3 h and transfected with Activator protein-1-Luc, Smad Binding Element (SBE)-Luc, or serial deletion mutants of human REDD1 promoter using Lipofectamine2000 reagent (Invitrogen) for 3 h. The phREDD1 and c-JUN plasmids were co-transfected in LX-2 cells. Next, cells were incubated in Dulbecco's modified Eagle's medium for 12 h. The firefly and renilla luciferase activities were measured using the dual luciferase assay system (Promega, Madison, WI, USA). Then, relative luciferase activities were calculated, as previously described (Shin et al. 2012).

Preparation of recombinant adenovirus

Recombinant adenoviruses expressing REDD1 or LacZ were produced in HEK293A cells, purified using $CsCl_2$, and resuspended in phosphate-buffered saline (PBS), as previously reported (Kim et al. 2015). Optical densities at 260 nm were measured to determine recombinant adenovirus titers.

Measurement of ROS production

After treatment with RSL3 or TGF-β in LX-2 cells, stained with 10 μM DCFH-DA for 1 h at 37°C. Fluorescence intensity in the cells was also measured using a fluorescence microplate reader (Gemini, Molecular Devices, Sunnyvale, CA, USA) at excitation/emission wavelengths of 485 nm/530 nm.

C11-BODIPY fluorescence analysis

After treatment with RSL3 in LX-2 cells, stained with 10 μM C11-BODIPY for 1 h at 37°C. Cells were then harvested by trypsinization and washed with PBS. The intensity of fluorescence in the cells was measured using flowcytometry (Beckman-Coulter). C11-BODIPY fluorescence was determined in channel FITC-A.

Animals

The protocols of all animal experiments were reviewed and approved by the Animal Care and Use Committee of Chosun University. Male ICR mice (6 weeks old) were purchased from Orient Bio (Sungnam, Korea) and acclimated for 1 week. Mice (N= 5 per group) were maintained at 25±2℃ under a 12 h light/dark cycle and a relative humidity of 50%±5% in filtered pathogen-free air with food (Purina, Korea) and water available *ad libitum*.

CCl_4-induced hepatic fibrosis

Adenovirus (1 x 10^8 pfu) were administered via a tail vein 48 h before CCl_4 injection and then once every 5 days for 2 weeks. To induce liver fibrosis, CCl_4 (0.5 mg/kg; dissolved in 10% corn oil) were intraperitoneally injected into the mice with two times a week for 2 weeks.

Iron dextran-induced hepatic ferroptosis

Mice were subjected to ferroptosis, as previously described (Zhang et al. 2013). To induce hepatic ferroptosis, Iron dextran (50 mg/kg; dissolved in saline) were intraperitoneally injected into the mice with once every day for 8-20 weeks.

Blood biochemistry

Plasma alanine aminotransferase (ALT) and aspartate aminotransferase (AST) levels were measured using commercial kits (Asan Pharmaceutical, Seoul, Korea).

TBARS assay

The relative malondialdehyde (MDA) contents in liver homogenates was quantified using the TBARS assay kit (STA-330; CELL BIOLABS, San Diego, CA, USA) according to the manufacturer's instructions.

Measurement of GSH content

The GSH contents in cells were quantified using a commercial GSH determination kit (BIOXYTECH GSH-400, Oxis International, Portland, OR, USA). Cells or liver tissues lysed in buffer containing 5% metaphosphoric acid to precipitate proteins. After centrifugation at 10,000×g for 15 min, the supernatants were used to measure GSH concentration. Absorbance at 400 nm was measured on a microplate reader (Spectra MAX, Molecular Device).

Measurement of GSH/GSSG ratio

GSH and GSSG ratio was quantified using the glutathione assay kit (703002; Cayman chemical, Ann Arbor, MI, USA) according to the manufacturer's instructions.

Histopathology and immunohistochemistry

Samples from ICR mouse hepatic tissues were crossly trimmed based on sagital axis, individually, and re-fixed in 10% neutral buffered formalin for 24 h. After embedded in paraffin using automated tissue processor and embedding center, 3-4 μm sections were prepared as three serial sections in each paraffin block using microtome. Representative sections were stained with hematoxylin and eosin (H&E) for general histopathological profiles, Sirius red (SR) for collagen fiber, Prussian blue (PB) for iron depositions, or Avidin-biotin- peroxidase complex (ABC)-based immunohistochemistry against α-smooth muscle actin (α-SMA) for activated hepatic stellate cells (HSCs). All histomorphometric and immunohistochemical analyses were conducted using automated digital image analysis software (DMI-300 Image processing; DMI, Daegu, Korea). Hepatocytes showing any degenerative changes including necrosis, eosinophilic condensation, acute cellular swelling (ballooning), iron depositions and fatty changes were regarded as "degenerative hepatocytes" under H&E and PB stain, and hepatic architectural changes, fibrosis and cirrhosis were evaluated by modified hepatic staging scoring system. In addition, the cells occupied by over 20% of immunoreactivities were regarded as positive. This analysis was conducted by a certified histopathologist unaware of sample identities.

Statistical analysis.

One-way analysis of variance (ANOVA) was used to assess statistical significance of differences among treatment groups. For each statistically significant effect of treatment, the Newman–Keuls test was used for comparisons between multiple group means. The data were expressed as means ± S.E.

III. RESULTS

Part I: The effect of ferroptosis in hepatic stellate cell activation

1. The effects of ferroptosis-inducers in hepatic stellate cells

First, we measured cell viability to investigate whether ferroptosis occurs in hepatic stellate cells (HSC). Cell viability was reduced by erastin or RSL3 in LX-2 cells. In another hepatic stellate cell lines, HSC-T6, the cell viability was also decreased by treatment with RSL3 (Fig. 1A). Erastin and RSL3 are well known as ferroptosis inducers. RSL3-induced cytotoxicity was significantly restored by deferoxamine (iron chealator) or ferrostatin-1 (ferroptosis inhibitor) in LX-2 cells. In HSC-T6 and in primary hepatic stellate cell isolated from mice, cell viability was also restored by ferrostatin-1 treatment (Fig. 1B). In contrast, other forms of cell death inhibitors such as, ZVAD-FMK (an apoptosis inhibitor), necrostatin-1 (Nec-1, a necroptosis inhibitor), and chloroquine (autophagy inhibitor) failed to restore cell viability following RSL3 treatment (Fig. 1C). Moreover, protein levels of cleaved PARP and caspase-3, known as apoptosis markers, were not changed by RSL3 treatments (Fig. 1D). These results indicate that cell death induced by ferroptosis inducers in HSCs is dependent on ferroptosis.

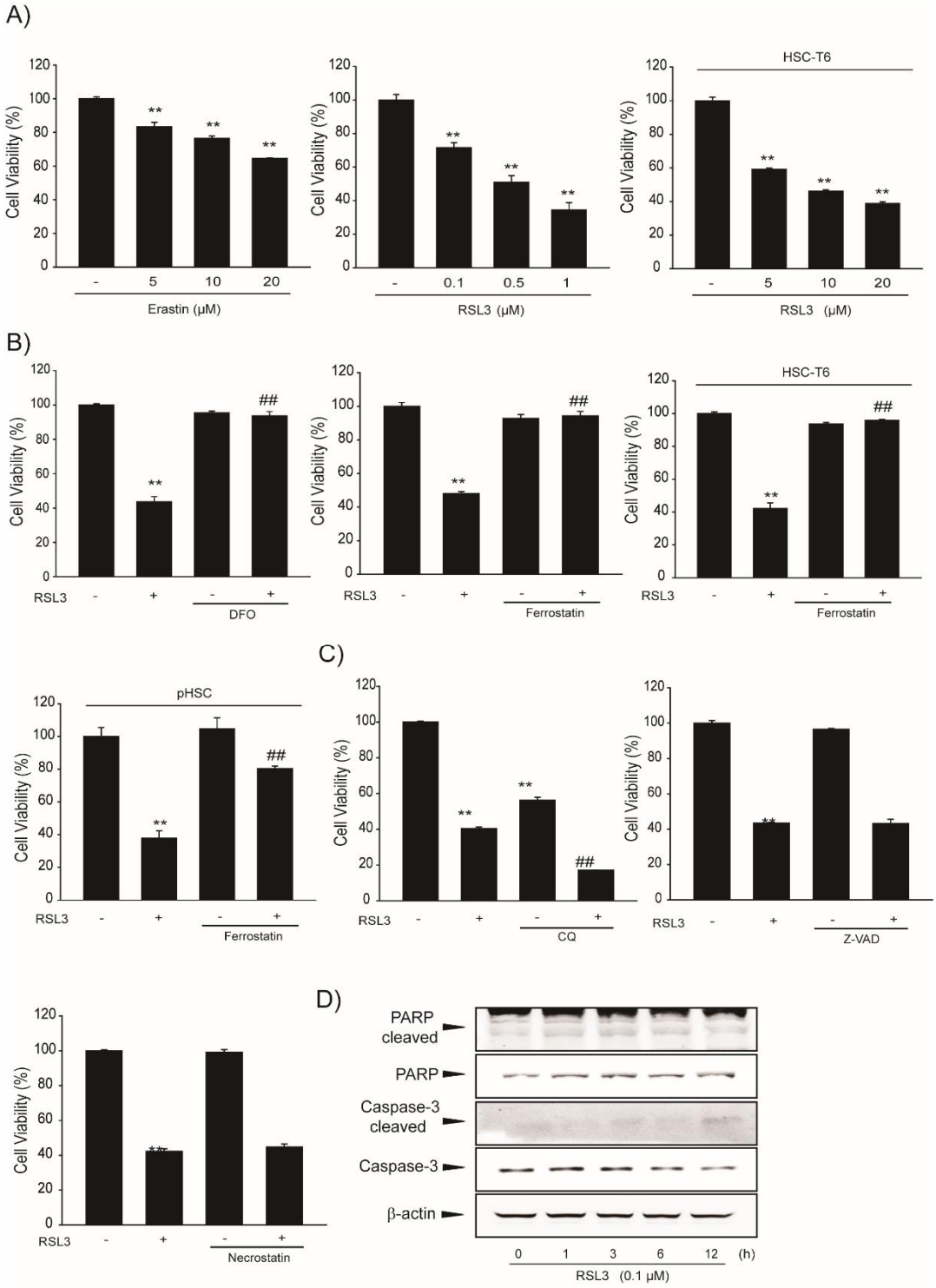

Figure 1. Induction of ferroptotic cell death in hepatic stellate cells (HSCs)

(A) Induction of cell death by ferroptosis-inducing compounds in hepatic stellate cells. LX-2 cells were treated with erastin or RSL3 for 24 h. Cell viabilities were assessed using an MTT assay. Data represent means ± S.E. of three replicates; significant as compared with vehicle treated control cells, **p<0.01 (B) The Effects of ferroptosis inhibitors on cell death induced by RSL3. Cells were treated with 100 μM of deferoxamine or 1 μM ferrostatin-1 with or without RSL3. Cell viabilities were assessed using an MTT assay. Data represent means ± S.E. of three replicates; significant as compared with vehicle treated control cells, **p<0.01, significant as compared with RSL3 treated control cells, ##p<0.01 (C) LX-2 cells were treated with RSL3 (0.1 μM) with or without the indicated inhibitors for 24 h. Cell viabilities were assessed using an MTT assay. Data represent means ± S.E. of three replicates; significant as compared with vehicle treated control cells, **p<0.01, significant as compared with RSL3 treated control cells, ##p<0.01 (D) Immunoblot of PARP, caspase3 and their cleaved forms in LX-2 cell from lysates treated with RSL3 (0.1 μM).

2. Identification of ferroptosis marker in HSCs

To verify that RSL3 has effects on human hepatic stellate cell line, we measured GPX4 protein level in LX-2 cells (Fig. 2A). GPX4 expression was reduced by RSL3 treatment. GPX4 reduction is a representative marker of ferroptosis. But, GPX1 expression was not significant. GPX1 is one of the GPX family, consisting of eight members. GPX1 is widely expressed in various tissues and protects cells against oxidative stress (Brigelius-Flohe and Maiorino 2013). In particular, GPX1 protects hemoglobin of erythrocytes from oxidative degradation or plays a crucial role of the arachidonic acid metabolism in platelets (Sutherland et al. 2001). However, GPX4 is known to play a more critical role than other GPX family members in ferroptosis (Yu et al. 2017). We next treated LX-2 cells with various time course of RSL3 to assess changes in the GSH/GSSG ratio. As a result, the GSH/GSSG ratio was decreased after treatment with RSL3 for 24 h (Fig. 2B). Dysfunction of intracellular antioxidant systems, such as GPX4 inactivation and GSH depletion, can affect ROS production. So, we measured intracellular ROS production using DCFH-DA fluorescence dye. Treatment of RSL3 for 3 to 6 h in LX-2 cells significantly increased ROS levels (Fig. 2C). Furthermore, RSL3 promoted the production of lipid ROS, one of the representative ferroptosis markers in LX-2 cells (Fig. 2D). To investigate the effect of RSL3 to iron metabolism in HSC, we measured the expression of iron transport related proteins transferrin receptor-1 (TfR-1) and ferroportin using immunoblotting. RSL3 treatment reciprocally regulates TfR-1 and ferroportin expression (Fig. 2E). To establish our finding that occuring ferroptosis in hepatic stellate cells, GPX4 expression was examined in murine primary hepatic stellate cells. When GPX4 expression was reduced, the HSC activation marker plasminogen activator inhibitor-1 (PAI-1) was increased by RSL3 or Fe-NTA

treatment. These results indicate that ferroptosis in HSCs can affect the hepatic stellate cell activation.

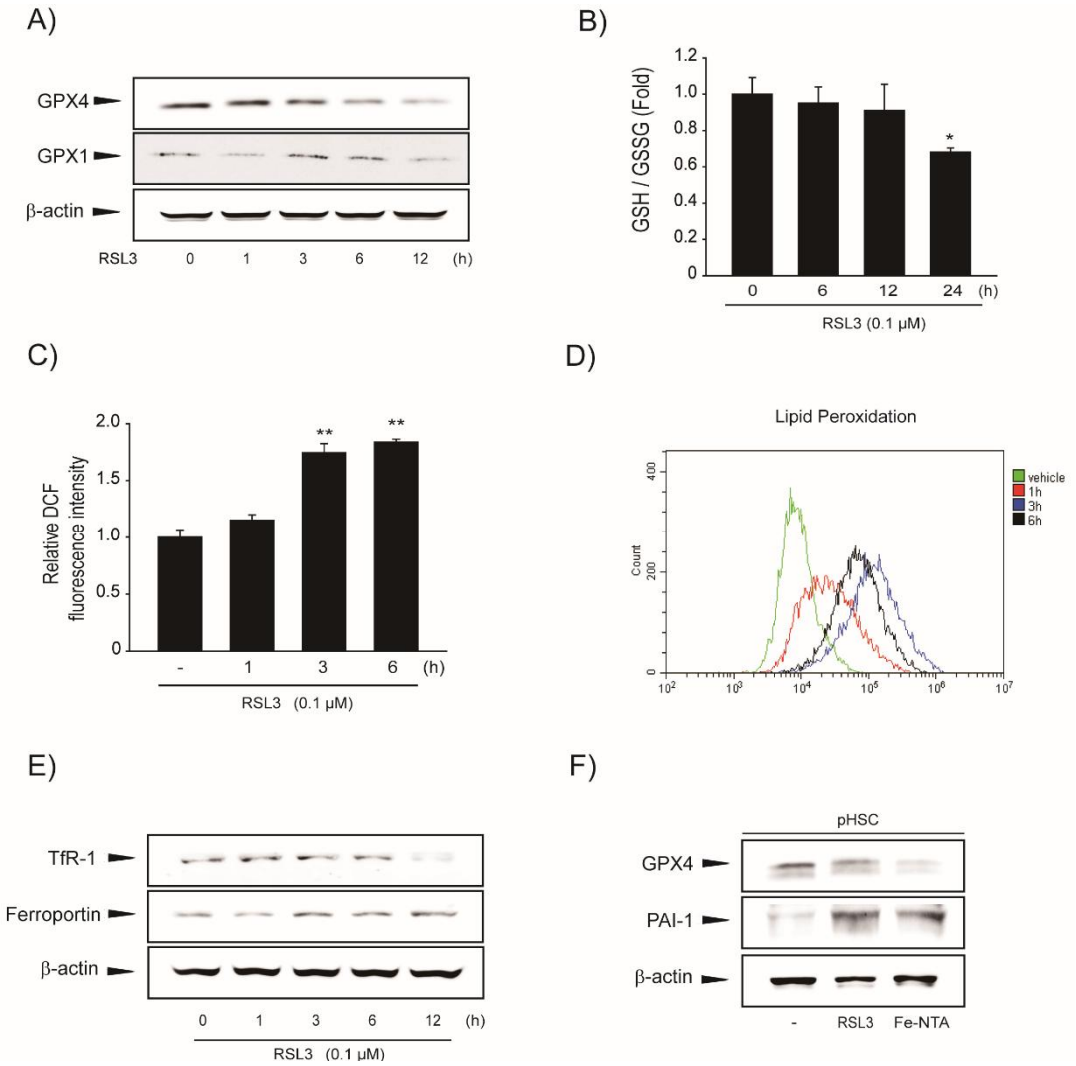

Figure 2. Characterization of ferroptosis in HSCs

(A) Protein levels of GPX4 or GPX1 in RSL3 (0.1 μM) treated LX-2 cells were measured by immunoblotting. (B) GSH/GSSG ratio was measured in lysates of LX-2 cells treated with RSL3 for various time course. Data represent means ± S.E. of three replicates; significant as compared with vehicle treated control cells, *$p<0.05$ (C) Cells were treated with RSL3 for 1-6 h. Then, we measured fluorescence intensities using DCFH-DA. Data represent means ± S.E. of three replicates; significant as compared with vehicle treated control cells, **$p<0.01$ (D) Lipid peroxidation by RSL3 in LX-2 cells. Fluorescence intensities of C11-bodipy were estimated after treatment with RSL3 (0.1 μM). (E) The effects of RSL3 on iron transport-related gene expression. Cells were treated with RSL3 in various time course. Protein levels were measured by immunoblotting. (F) Protein levels of GPX4 or PAI-1 in primary HSCs. After isolation of primary HSCs (day 0), the cells were treated with RSL3 (0.1 μM) or Fe-NTA (50 μM). Expression of the HSC activation marker PAI-1 and ferroptosis marker GPX4 was determined by immunoblot analysis.

3. Ferroptosis-inducers contribute to HSC activation

To investigate whether ferroptosis-inducers contribute to fibrogenic gene expression, we treated RSL3 or Fe-NTA in LX-2 cells. RSL3 or Fe-NTA treatment in LX-2 cells increased the expression of PAI-1 protein expression (Fig. 3A). In HSCs, PAI-1 plays a crucial role in the synthesis and secretion of ECM proteins (Knittel et al. 1996). Therefore, PAI-1 is considered a representative HSC activation marker. Next, we observed that tissue inhibitor of metalloproteinases-1 (TIMP-1) or PAI-1 mRNA expression was affected by RSL3. PAI-1 or TIMP-1 mRNA level was increased by RSL3 treatment for 1-3 h (Fig. 3B). It is known that upregulation of TIMP-1 indirectly promotes ECM accumulation (Arpino et al. 2015). Treatment with ferrostatin-1, a specific inhibitor of ferroptosis, completely inhibited the increase in PAI-1 levels induced by RSL3 (Fig. 3C). These data suggest that ferroptosis can contribute to HSC activation.

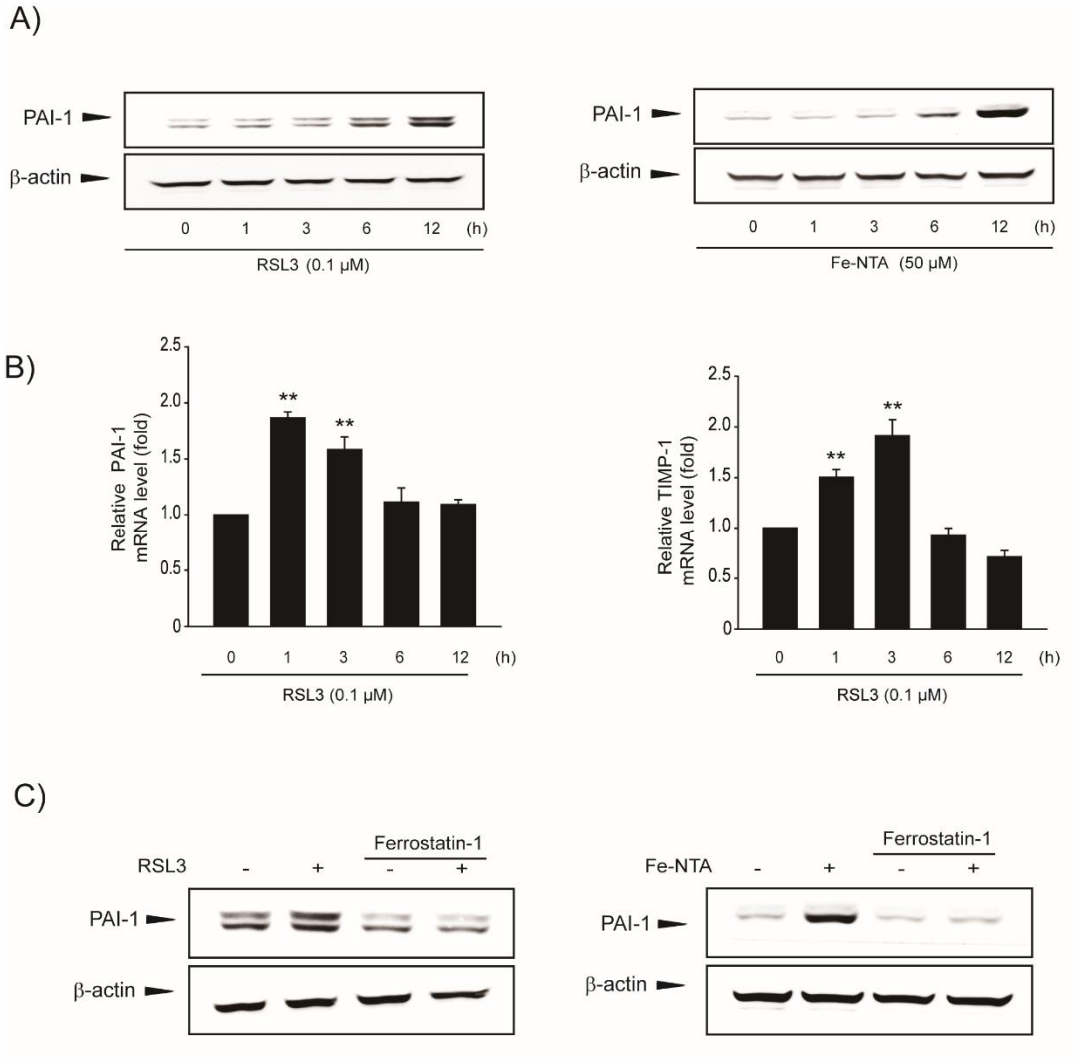

Figure 3. HSC activation by ferroptosis-inducing compounds

(A) Cells were treated with RSL3 or Fe-NTA for 1-12 h. Then, PAI-1 protein level was determined by immunoblotting. (B) Real-time PCR analysis. Cells were treated with RSL3 for 1-12 h. PAI-1 or TIMP-1 mRNA levels were normalized as using GAPDH. Data represent means ± S.E. of three replicates; significant as compared with vehicle treated control cells, *$p<0.05$, **$p<0.01$ (C) LX-2 cells were exposed to RSL3 (0.1 μM) or Fe-NTA (50 μM) for 6 h after pretreatment with ferrostatin-1 for 30 min. PAI-1 protein level was measured by immunoblotting.

4. AP-1-dependent HSC activation by ferroptosis inducers

Activator protein 1 (AP-1) is a transcription factors consisting of Jun, Fos or Activating Tanscription Factor (ATF) protein (Gangnuss et al. 2004). In addition, it has been reported that AP-1 is a major redox-sensitive transcription factor (Korashy and El-Kadi 2008) and regulate genes involved in TIMP and ECM remodeling (Li et al. 2008). Based on Fig. 2C and 3B, we speculated that AP-1 could involve in HSC activation by RSL3. Therefore, we measured AP-1 luciferase activity to determine the signaling pathway involved the HSC activation by RSL3. Treatment with RSL3 elevated AP-1 luciferase activity in a dose-dependent manner (Fig. 4A). Next, we treated LX-2 cells with various time course of RSL3 to assess the c-JUN phosphorylation, which is major component of AP-1. An immunoblot results showed that phosphorylation of c-JUN was increased by RSL3 (Fig. 4B). Phosphorylated-c-JUN increased by RSL3 or Fe-NTA was completely abolished by treatment with the ferroptosis inhibitor ferrostatin-1 (Fig. 4C and 4D). However, Smad pathway, the major signaling in HSC activation, has not been affected by RSL3 or Fe-NTA. Result for investigating Smad phosphorylation by RSL3 in LX-2 cells, both Smad2 or Smad3 phosphorylation has not changed (Fig. 4E). Then, we also measured Smad-binding element (SBE)-dependent luciferase activity. In agreement with immunoblotting data, SBE luciferase activity was not increased by RSL3 treatment (Fig. 4F). These data indicate that ferroptosis-inducers contribute to HSC activation via AP-1-dependent pathway, not Smad signaling pathway.

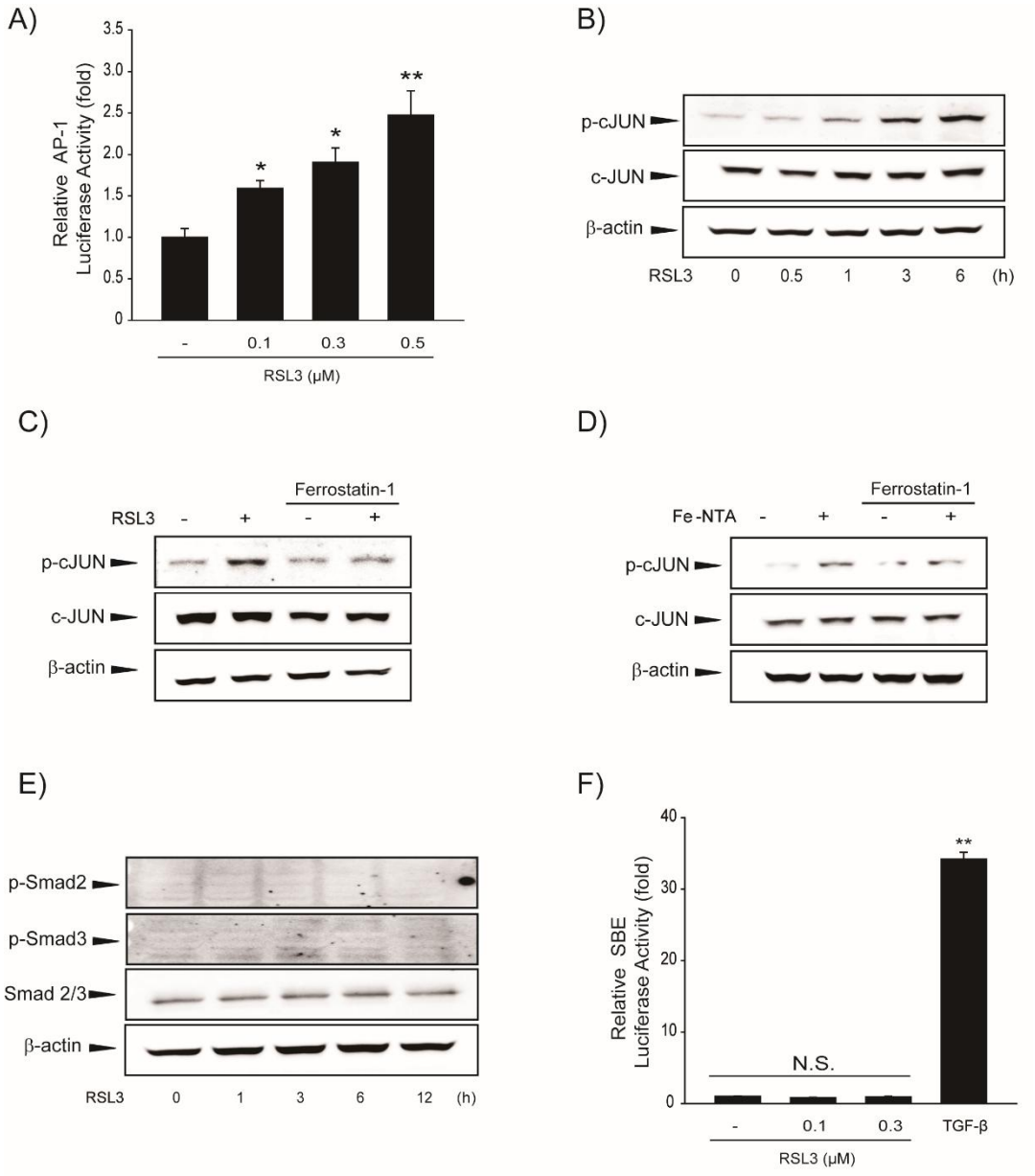

Figure 4. AP-1-dependent ferroptosis in HSCs

(A) AP-1-luciferase activity was determined in the lysates of LX-2 cells treated with RSL3 for 12 h. Data represent means ± S.E. of three replicates; significant as compared with vehicle treated control cells, *$p<0.05$, **$p<0.01$ (B) Immunoblot analysis for phosphorylated c-JUN was carried out in cells treated with RSL3 (0.1 μM) for 0.5–6 h. (C) Cells were exposed to RSL3 (0.1 μM) for 6h after pretreatment with ferroptstatin-1 (1 μM) for 30 min. Then, phosphorylated c-JUN protein level was measured immunoblotting. (D) LX-2 cells were pretreated as described in (C) and treated with Fe-NTA (50 μM) for 6 h. Protein level of phosphorylated c-JUN was determined by immunoblotting. (E) LX-2 cells were treated with 0.1 μM of RSL3 in various time course. And the phosphorylation levels of Smad2 or Smad3 were analyzed. (F) Smad transactivation was measured in LX-2 cells transfected with the SBE luciferase construct and exposed to RSL3 for 12 h. TGF-β treated cells were used as positive control. Data represent means ± S.E. of three replicates; significant as compared with vehicle treated control cells, **$p<0.01$

5. Activation of the HSC induces ferroptosis

First, we investigated the GPX4 expression in primary hepatic stellate cells. GPX4 protein level was decreased in activated HSC (Fig. 5A). Then, we treated TGF-β in LX-2 cells with various time course. GPX4 protein levels were decreased after TGF-β treatment for 12 h or 24 h (Fig. 5B). Treatment of ferrostatin abolished the reduced GPX4 expression by TGF-β (Fig. 5C). Next, we measured reactive oxygen species (ROS) production in LX-2 cells after TGF-β treatment using DCFH-DA. It has been well established that ROS generation in HSCs is critical for liver fibrosis progression (Parola and Robino 2001). In addition, elevated ROS levels are commonly detected in liver fibrosis model (Svegliati Baroni et al. 1998). ROS also plays an important role in the ferroptosis occurrence (Xie et al. 2016). ROS production was significantly increased for 6-12 h in LX-2 cells by TGF-β treatment (Fig. 5D). These results suggest that ferroptotic conditions may occur during HSC activation by TGF-β treatment.

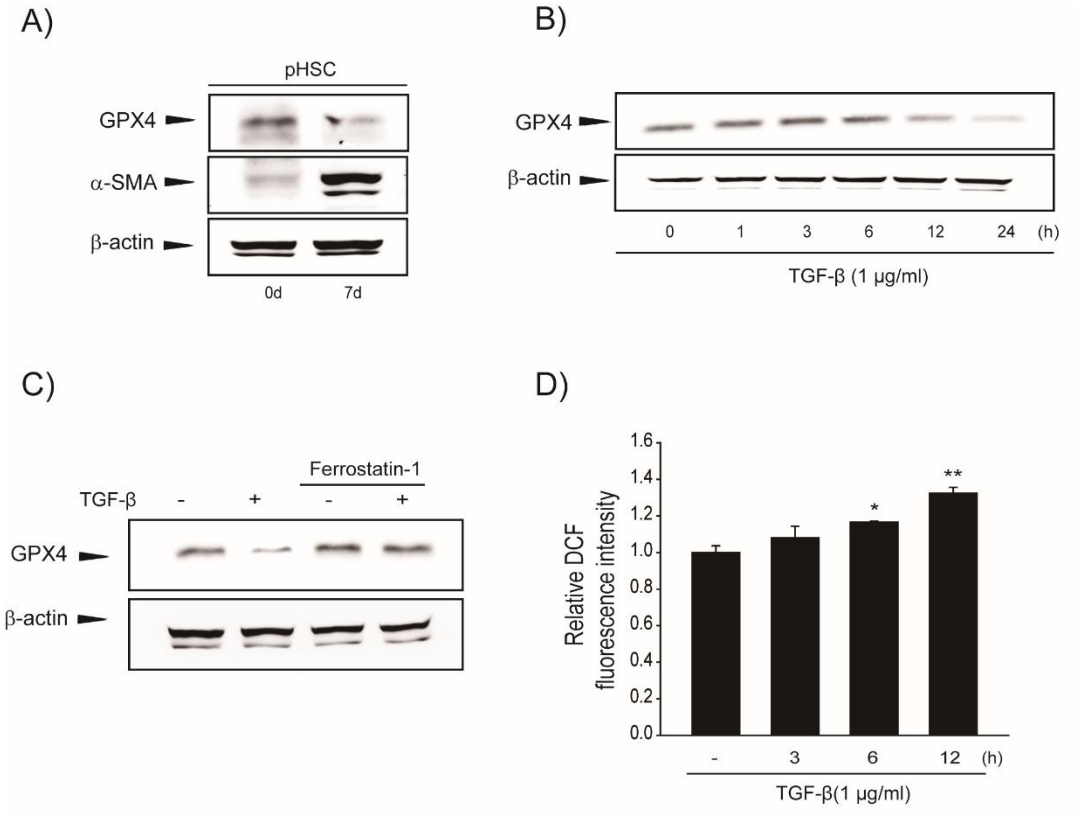

Figure 5. TGF-β activates HSC by inducing ferroptotic condition

(A) Immunoblotting on quiescent or activated primary HSCs. After primary HSCs isolated from mice (day 0), the cells were incubated for 7 days, and the cell lysates were used to immunoblotting. (B) Immunoblot analyses for GPX4 were carried out in cells treated with TGF-β (1 μg/ml) for 1–24 h. (C) ROS production by TGF-β in LX-2 cells. Intracellular fluorescence intensities of DCFH-DA were estimated after treatment with TGF-β (1 μg/ml) for 3-12 h. Data represent means ± S.E. of three replicates; significant as compared with vehicle treated control cells, *$p<0.05$, **$p<0.01$

6. Iron dextran-induced liver injury

Previous reports showed that chronic administration of iron-dextran induced hepatic injury (Zhang et al. 2013). To explore whether iron dextran administration promoted liver fibrosis, we intraperitoneally injected iron dextran to mice for 8-20 weeks at a dose of 50 mg/kg daily. First, we performed blood biochemistry analysis. ALT and AST levels, serum markers commonly used for liver damage, and they were significantly increased in all iron-dextran treated groups (Fig. 6A). In hematoxylin and eosin (H&E) staining for general histopathology, pathological changes such as focal hepatocellular necrosis, acute cellular swelling (ballooning), eosinophilic condensation, deposit of lipid droplets (fatty changes) and inflammatory cell infiltrations were observed form 8 weeks after iron-dextran administration (Fig. 6B). These results indicate that iron dextran administration induced obvious liver injury.

A)

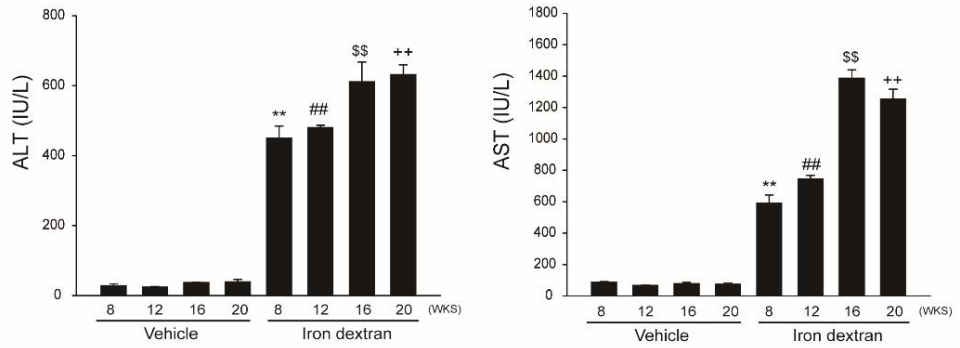

B)

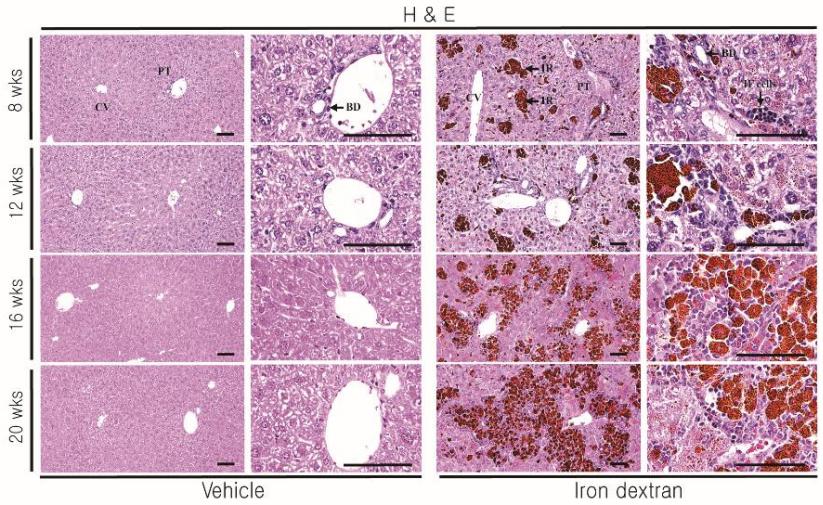

Figure 6. Iron dextran-induced liver damage

(A) ALT and AST activities in iron dextran-induced mice serum (*N* = 3 or 5). All values are determined using commercial kits. Results are presented as mean ± S.E significant as compared with each vehicle treated control group, $^{**}p < 0.01$, $^{\#\#}p < 0.01$, $^{\$\$}p < 0.01$, $^{++}p < 0.01$ (B) Representative histological sections of the liver. Samples were stained with H&E for general histological observations (Scale bars indicate 120 μm). CV, central vein; PT, portal triad; BD, bile duct.

7. Iron dextran-induced hepatic ferroptosis

Next, we examined ferroptosis in a mouse model of chronic iron overload-induced hepatic fibrosis. Iron accumulation is one of the major features of ferroptosis (Dixon and Stockwell 2014). First, we measured MDA, the final product of lipid peroxidation, using TBARS assay. MDA levels were significantly increased in iron dextran-treated mice (Fig. 7A). Next, we investigated the GSH depletion in mice liver homogenates. Decrease of GSH was observed in the mice liver administered iron dextran for 8 to 12 weeks. However, GSH levels in iron dextran-treated mice liver for 16-20 weeks were unexpectedly increased (Fig. 7B). Furthermore, we assessed protein marker of ferroptosis in mouse liver. GPX4 protein levels were decreased in 12 weeks treated group, while it increased in 20 weeks treated group (Fig. 7C). Next, iron accumulation region was confirmed using Prussian blue staining. Iron accumulation increased markedly as the administration period was prolonged (Fig. 7D). These results suggest that iron overload induced ferroptosis in liver.

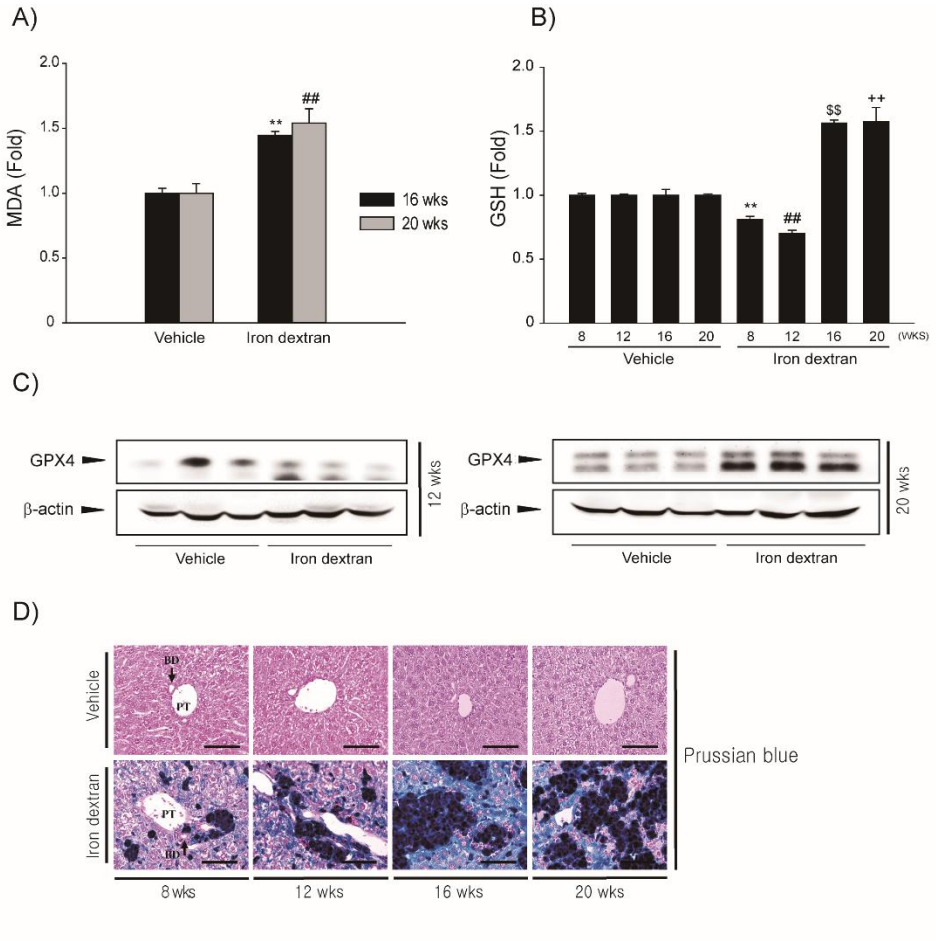

Figure 7. Iron overload in the liver induces ferroptosis

(A) Lipid peroxidation was measured by TBARS assay in liver homogenates. Results are presented as mean ± S.E. significant as compared with vehicle control, **$p < 0.01$, $^{\#\#}p < 0.01$; significant as compared with each vehicle treated group. (B) GSH contents was measured using commercial kits in liver homogenates. Results are presented as mean ± S.E. significant as compared with vehicle control, **$p < 0.01$, $^{\#\#}p < 0.01$, $^{\$\$}p < 0.01$, $^{++}p < 0.01$; significant as compared with each vehicle treated group. (C) GPX4 expression by treatment of iron dextran for 12 or 20 weeks in mouse liver. Protein levels were evaluated by immunoblot analysis. (D) Prussian blue staining in liver tissues treated with iron dextran (Scale bars=120 μm).

8. Iron dextran-induced liver fibrosis

To investigate whether iron dextran administration induces liver fibrosis, we assessed protein marker of fibrosis in mouse liver. Expression of fibrosis markers, α-SMA and PAI-1, were increased in both 12- or 20-weeks treatment groups (Fig. 8A). Moreover, collagen fiber deposition was confirmed using Sirius Red staining. Collagen accumulation was markedly increased as the administration period was prolonged (Fig. 8B). Immunohistochemistry presented that the numbers of α-SMA (activated HSCs marker)-positive cells were significantly increased in hepatic tissue from mice injected with iron dextran (Fig. 8C). More than 30% of the collagen fiber occupied area and mean over 100 of α-SMA positive cell numbers were observed from 20 weeks after iron dextran injection. These findings suggest that iron overload-induced ferroptosis contributes to hepatic fibrosis.

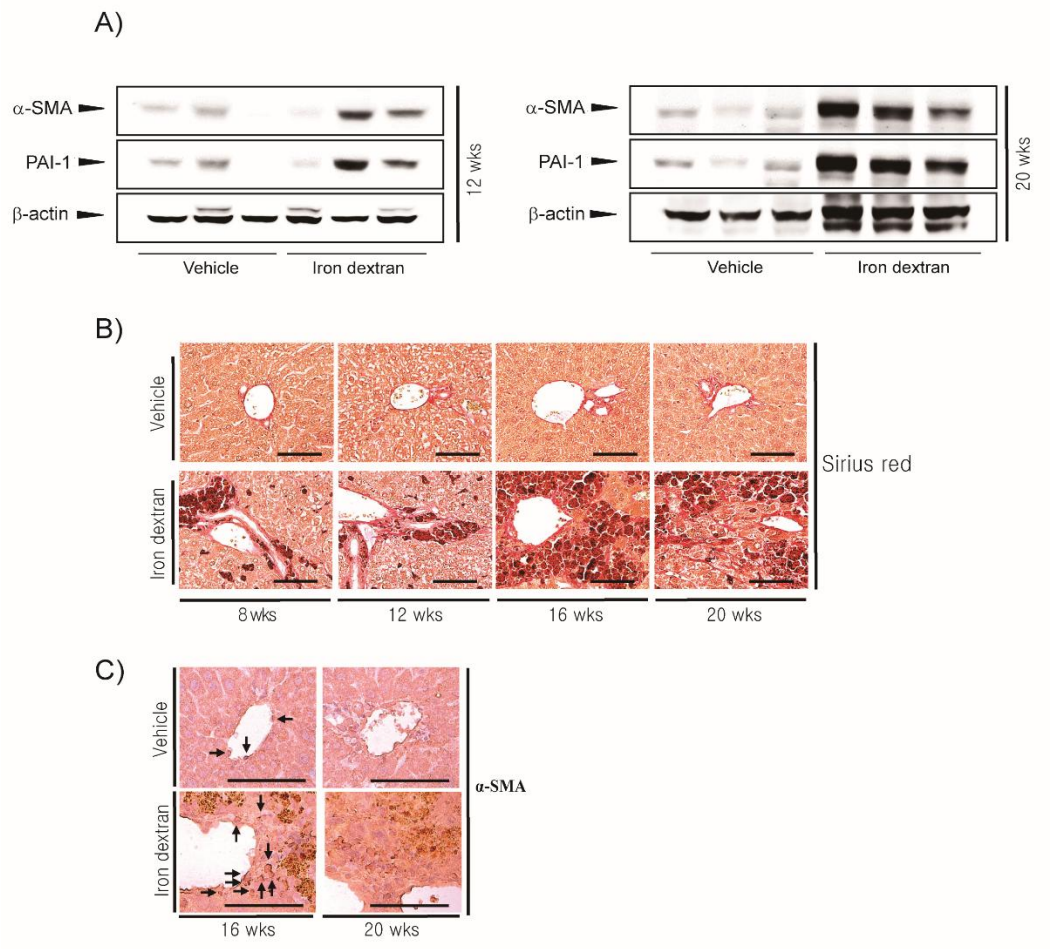

Figure 8. Liver fibrosis induced by chronic iron overload

(A) Immunoblot analysis for α-SMA and PAI-1 was carried out in mouse liver homogenates induced for 12 or 20 weeks with iron dextran. (B) Representative histological sections of the liver. Samples were stained Sirius Red (C) Immunohistochemical staining of α-SMA in liver from mice injected with iron dextran (Scale bars=120 μm).

.

Table 2. Histomorphometrical analysis of hepatic tissues, taken from vehicle or iron dextran-treated mice

Index	General histomorphometry						Mean α-SMA immunoreactive cell numbers (cells/mm^2)
Group	Hepatic Staging Scores (Max = 10)*	Percentages of DE regions (%/mm^2)	DE hepatocytes (cells/1000 hepatocytes)	Inflammatory cells infiltrated (cells/mm^2)	Collagen fiber occupied regions (%/mm^2)	Iron deposition occupied regions (%/mm^2)	
Sampled at 8 weeks after treatment							
Vehicle	0.20±0.42	2.44±1.88	19.00±16.93	22.20±10.93	1.54±0.72	0.00±0.00†	
Iron dextran	1.70±0.48[a]	70.25±11.72[a]	676.60±120.89[a]	185.40±59.28[a]	5.73±1.27[a]	18.92±11.71[a]	
Sampled at 12 weeks after treatment							
Vehicle	0.30±0.48	2.53±2.97	21.00±24.72	48.20±19.03	1.89±1.08	0.00±0.00	
Iron dextran	2.20±0.92[a]	76.75±11.72[a]	747.00±114.54[a]	208.20±54.19[a]	8.54±4.55[a]	35.59±12.08[a]	
Sampled at 16 weeks after treatment							
Vehicle	0.30±0.48	4.05±3.53	36.20±32.17	48.80±18.21	2.05±1.41	0.00±0.00	8.00±4.71
Iron dextran	3.00±0.82[a]	79.78±11.80[a]	777.60±117.36[a]	668.00±199.45[a]	15.39±8.02[a]	45.80±12.20[a]	80.80±20.98[a]
Sampled at 20 weeks after treatment							
Vehicle	0.40±0.52	4.44±4.17	36.90±39.33	42.60±20.48	2.16±0.89	0.00±0.00	10.60±6.19
Iron dextran	4.20±0.63[a]	85.20±10.08[a]	828.60±107.91[a]	816.70±181.57[a]	35.49±10.52[a]	60.19±13.97[a]	140.40±37.32[a]

Values are expressed as mean ± SD of 10 histological fields

* Details of hepatic staging scores

No fibrosis	0
Fibrous expansion of some portal areas, with or without short fibrous septa	1
Fibrous expansion of most portal areas, with or without short fibrous septa	2
Fibrous expansion of most portal areas with occasional P-P bridging	3
Fibrous expansion of portal areas with marked bridging P-P as well as P-C	4
Marked bridging (P-P and/or P-C) with occasional nodules (incomplete cirrhosis)	5
Cirrhosis, probable or definite	6

P-P = Portal to portal
P-C = Portal to central
Possible maximum total scores = 6
Modified from the method described by Ishak et al. 1995

† Not detected

DE = Degenerative; SMA = Smooth muscle actin

[a]$p<0.01$ as compared with vehicle treated mouse hepatic tissues, sampled at equal treatment periods by MW test

Part II: The role of REDD1 in liver fibrosis

1. REDD1 repression in fibrotic liver

In the pathogenesis of liver fibrosis, oxidative stress plays a pivotal role (Paik et al. 2014). Several studies previously demonstrated that antioxidant gene expressions are inversely related to liver fibrosis progression (Whalen et al. 1999). In addition, we recently reported that REDD1 could protect oxidative stress-mediated hepatocyte injury (Cho et al. 2018). Therefore, we first investigated the expression of REDD1 in ferroptosis-mediated liver fibrosis model by iron overload. The results obtained showed REDD1 expression was decreased in all iron dextran-treated groups (Fig. 9A). Based on these results, we hypothesized that REDD1 gene may affects the liver fibrosis progression.

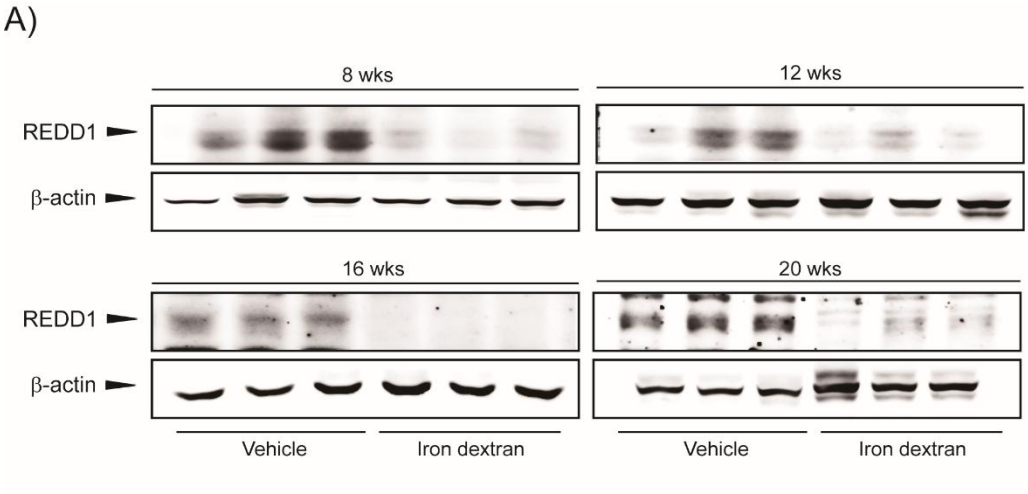

Figure 9. Inhibition of REDD1 in fibrotic liver

(A) REDD1 expression in mouse liver induced by iron dextran for 8-20 weeks. Protein levels were evaluated by immunoblot analysis.

2. Induction of REDD1 in activated HSCs

Initially, we examined the REDD1 expression in LX-2 cells. REDD1 protein levels were increased by TGF-β treatment and peaked at 3 h (Fig. 10A). Then, we treated LX-2 cell with various concentration of TGF-β. Likewise, an increased REDD1 protein levels were observed (Fig. 10B). To determine whether induction of REDD1 by TGF-β was transcriptional regulation, we performed RT-PCR analysis. we observed that REDD1 mRNA levels were increased by TGF-β treatment (Fig. 10C). And this increase was completely inhibited by RNA polymerase inhibitor, actinomycin-D (ActD) pretreatment (Fig. 10D). In addition, we measured the luciferase activity of human REDD1 promoter. TGF-β treatment significantly increased the REDD1 luciferase activity (Fig. 10E). Next, we investigated whether REDD1 gene expression was altered during activation of primary cultured murine HSCs. In activated HSCs, REDD1 protein levels were markedly increased in parallel with α-SMA protein levels, which is HSCs activation marker (Fig. 10F). These results suggest that TGF-β transcriptionally regulates REDD1 gene expression.

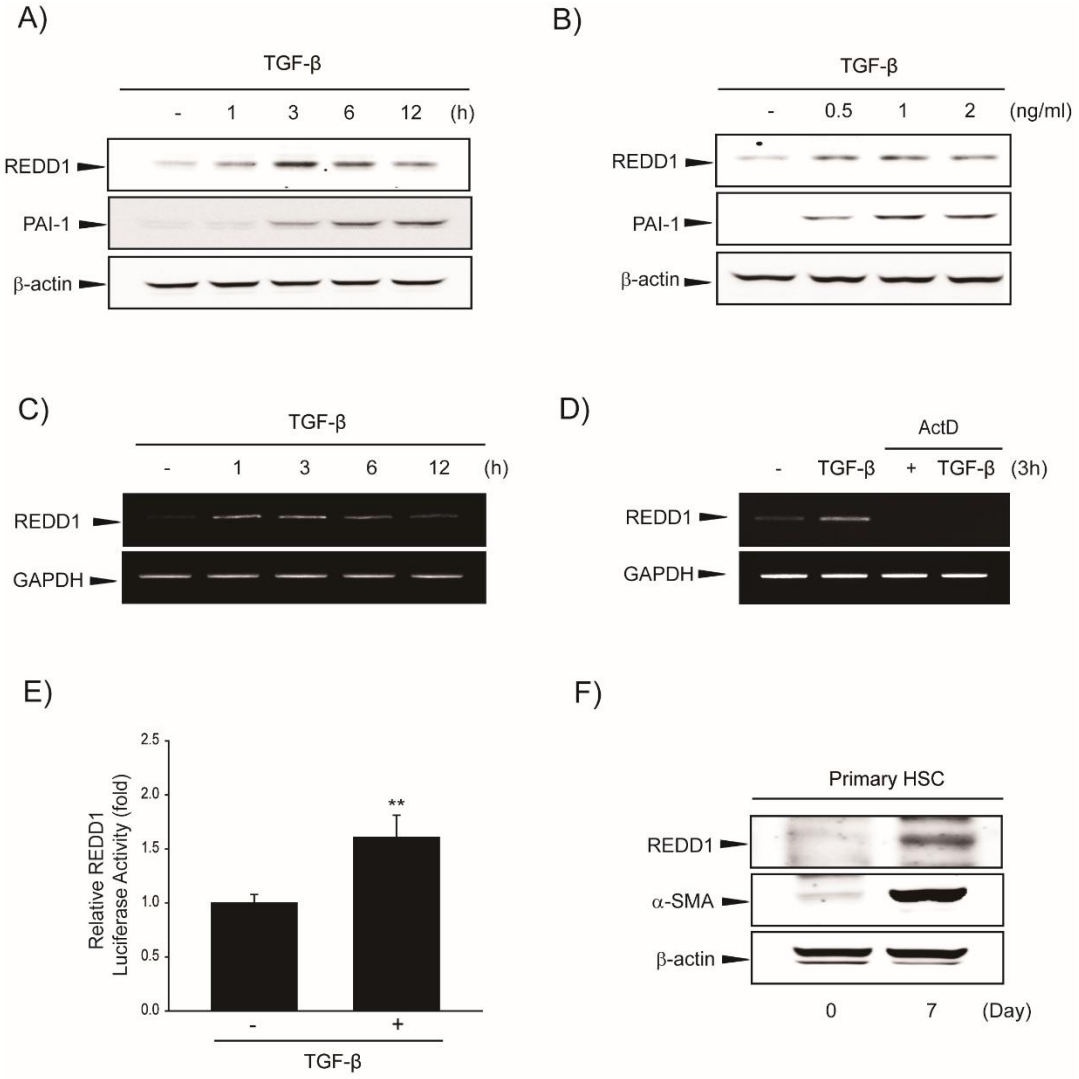

Figure 10. Upregulation of REDD1 during HSC activation

(A) LX-2 cells were treated with TGF-β (1 ng/mL) for 1-12 h. REDD1 or PAI-1 protein levels were measured by immunoblotting. (B) REDD1 or PAI-1 expression was determined in LX-2 cells treated with indicated concentration of TGF-β for 6 h. (C) Cells were treated with 1 ng/mL TGF-β for 1–12 h. Then, REDD1 mRNA levels were determined by RT-PCR analysis. (D) The cells were treated with 5 μg/mL of ActD in the presence or absence of TGF-β. REDD1 mRNA level was detected after TGF-β treatment for 3 h. (E) REDD1 luciferase activity was measured in the lysates of LX-2 cells treated with TGF-β for 12 h. Data represent means ± S.E. of three replicates; significant as compared with vehicle treated control cells, **$p<0.01$ (F) REDD1 expression in primary HSCs. After primary HSCs isolation from mice (day 0), cells were cultured for 7 days, and the cell lysates were subjected to immunoblotting.

3. AP-1 dependent REDD1 induction by TGF-β

TGF-β signals were mainly through the Smad pathway, and activated Smad proteins regulate cellular functions by involving in the expression of various genes (Massague 2012). So, we explored the role of Smad in TGF-β-mediated REDD1 induction. LX-2 cells were transfected with a plasmid expressing Smad3. But, Smad3 overexpression did not affect the REDD1 expression (Fig. 11A). Also, similar results were observed in the REDD1 reporter gene analysis. We co-transfected cells with Smad3 and REDD1 luciferase reporter gene. Consistently, REDD1 luciferase activity was not changed by Smad3 transfection (Fig. 11B). It was well known that TGF-β contributes to ROS or RNS in injured liver (Parola and Robino 2001). In addition, ROS activates HSC by acting as an intracellular signaling mediator of the pro-fibrogenic effect of TGF-β (Poli 2000). Previously, we reported that ROS-mediated REDD1 induction is dependent on AP-1 activation (Cho et al. 2018). Therefore, we first confirmed that REDD1 expression was increased by c-JUN overexpression (Fig. 11C). In agreement with previous our report, REDD1 luciferase activity was also increased by c-JUN overexpression (Fig. 11D). To investigate the effect of TGF-β on c-JUN activation, we treated LX-2 cells with TGF-β in various time-courses. Phosphorylation of c-JUN was increased by TGF-β treatment (Fig. 11E). AP-1 luciferase activity was also increased by TGF-β (Fig. 11F). These results suggest that TGF-β-mediated REDD1 induction is dependent on AP-1, but not Smad. TGF-β signaling can activate not only Smad but also other molecules including MAPK (Gui et al. 2012). To determine the role of MAPKs in REDD1 induction by TGF-β, we pretreated cells with MAPKs inhibitors. We found that REDD1 induction was completely inhibited by the p38 inhibitor (Fig. 11G).

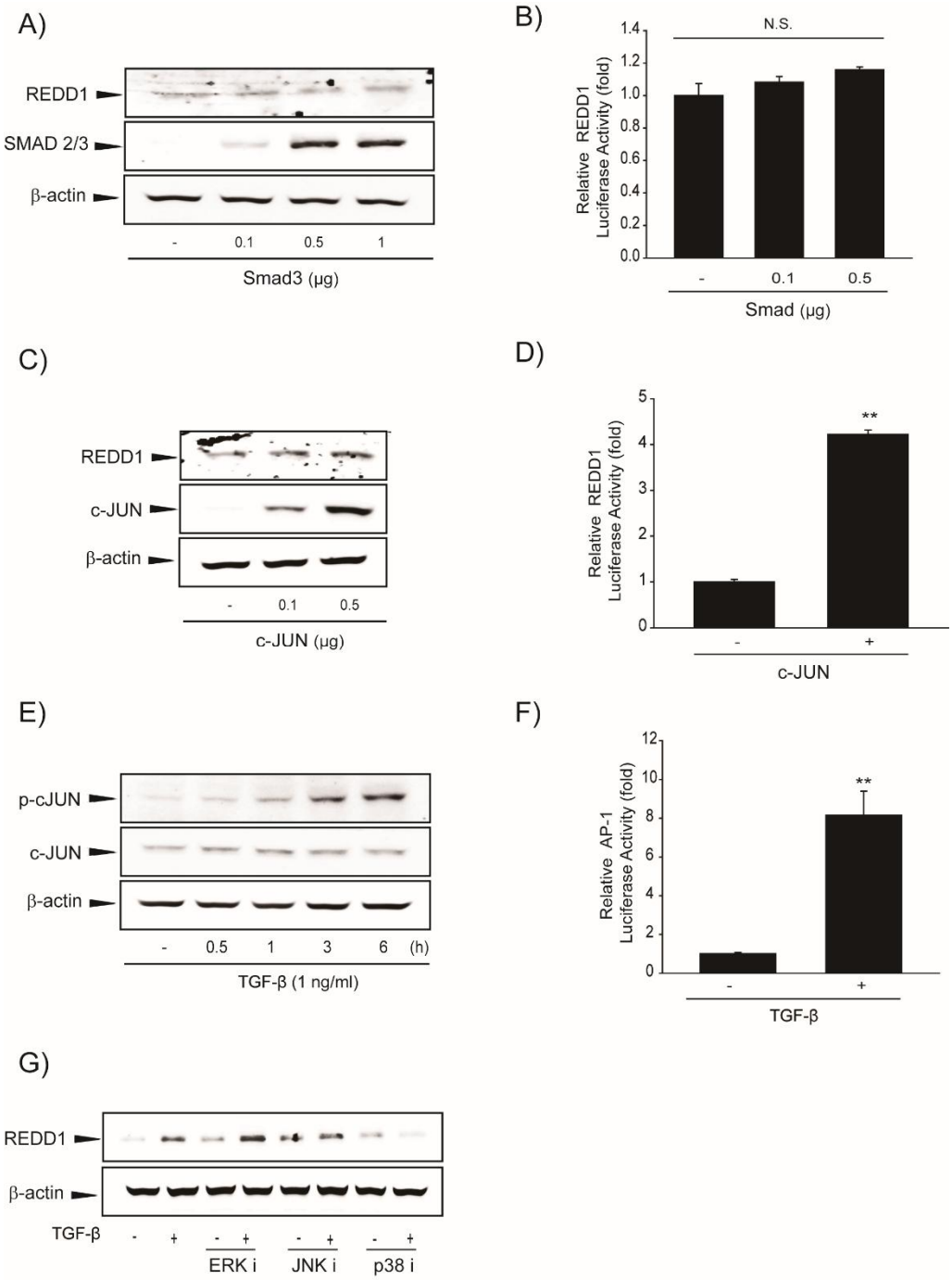

Figure 11. AP-1-dependent REDD1 induction in HSCs

(A) Cells were transfected with a plasmid DNA expressing Smad3 for 24 h. Then, the protein levels of REDD1 and Smad2/3 in cells were evaluated by immunoblotting. (B) Cells were co-transfected with plasmid DNA that expresses Smad3 and REDD1 promoter containing reporter gene. Data represent means ± S.E. of three replicates; significant as compared with MOCK transfected cells, N.S., not significant. (C) LX-2 cells were transfected with a c-JUN expression construct. REDD1 or c-JUN protein levels were determined by immunoblotting (D) LX-2 cells were transfected with plasmids expressing c-JUN and REDD1 luciferase reporter gene. Then, reporter assay was carried out in the lysates of cells. Data represent means ± S.E. of three replicates; significant as compared with vehicle treated control cells, **$p<0.01$ (E) The effect of TGF-β treatment on c-JUN phosphorylation. LX-2 cells were treated with 1 ng/mL TGF-β. c-JUN phosphorylation level in the cell lysates were measured by immunoblotting. Data represent means ± S.E. of three replicates; significant as compared with vehicle treated control cells, **$p<0.01$ (F) AP-1 luciferase activity was measured from the lysates of LX-2 cells exposed to TGF-β. (G) Cells were exposed to TGF-β (1 ng/mL) for 6 h after pretreatment with mitogen-activated protein kinase (MAPK) inhibitors. REDD1 protein levels were measured by immunoblotting.

4. Role of putative AP-1 binding site in TGF-β-mediated REDD1 induction

REDD1 induction

As previously described (Cho et al. 2018), we found 20 putative AP-1 binding sites in human REDD1 promoter. Then, we constructed human REDD1 promoter which sequentially deleted AP-1 binding site. To determine the essential binding site of AP-1 by TGF-β, we measured the luciferase activities with TGF-β treatment in each serially deleted promoter. The luciferase activity of phREDD1-2548 in LX-2 cells was significantly increased by TGF-β treatment. phREDD1-1271 or -716 luciferase activities were also significantly increased. However, luciferase activity increase by TGF-β was completely abolished in phREDD1-587 transfected cells (Fig. 12A). In our previous study, it was found that one AP-1 binding site was present at -716 to -589 bp of the human REDD1 promoter (Cho et al. 2018). We deleted the only AP-1 binding site left in phREDD1-716, and conducted reporter gene assay. Specific deletion of AP-1 binding site in phREDD1-716 was abolished the luciferase activity that increased by TGF-β treatment in phREDD1-716 promoter (Fig. 12B). These results indicated that AP-1 plays an essential role in REDD1 induction by TGF-β.

A)

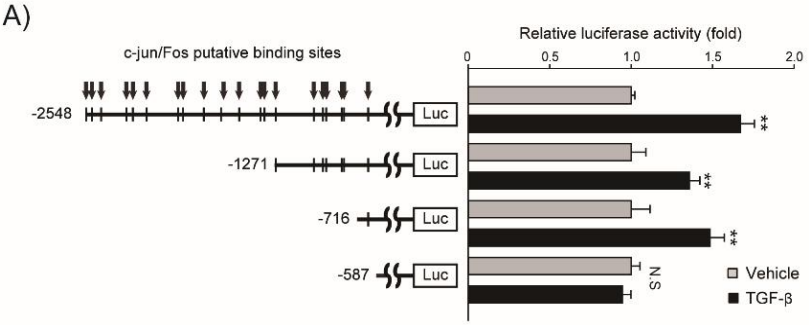

B)

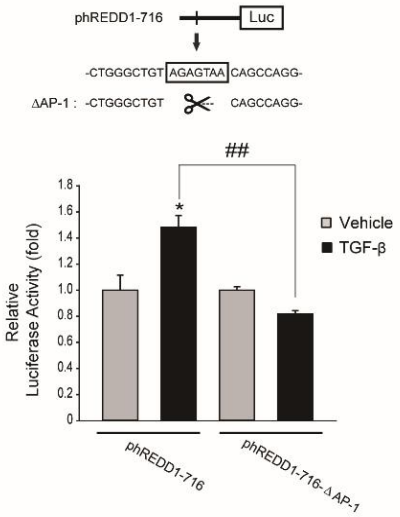

Figure 12. The key site of AP-1 binding in TGF-β-mediated REDD1 induction

(A) Schematic illustration of phREDD1 plasmids. Arrows indicate putative AP-1 binding sites in human REDD1 promoter (left). Cells were transfected with sequentially deleted phREDD1 plasmids for 24 h. Then, reporter gene assay was performed in the lysates of cells exposed to TGF-β (right). (B) LX-2 cells were transfected with phREDD1-716-ΔAP-1 plasmid. The phREDD1-716-ΔAP-1 is a promoter which proximal AP-1 binding site is deleted in phREDD1-716. After transfection, cells were treated with TGF-β (1 ng/ml) for 12 h. Then, reporter gene assay was performed in cell lysates.

5. The role of REDD1 in TGF-β-dependent Smad activation

Next, we investigated the role of REDD1 on Smad phosphorylation and fibrogenic gene expression by TGF-β. PAI-1 expression was increased by TGF-β treatment in Ad-LacZ infected LX-2 cells, but this effect was diminished in Ad-REDD1 infected cells (Fig. 13A). To elucidate the correlation between REDD1 and TGF-β signaling, we examined the role of REDD1 on Smad phosphorylation. Treatment of LX-2 cells with TGF-β increased phosphorylation of Smad3. However, REDD1 overexpression using Adenovirus infection inhibited the Smad3 phosphorylation (Fig. 13B). Furthermore, REDD1 overexpression increased Smad7 expression (an inhibitory factor) (Fig. 13C). These results indicate that REDD1 has an anti-fibrotic effect by inhibiting TGF-β-mediated Smad3 phosphorylation and increasing Smad7 expression. To explain the anti-fibrotic effect of REDD1, we investigated several molecules that might be involved. Recently, it has been reported that liver fibrosis can be ameliorated through mTOR inhibition by increasing AMPK activity (Wu et al. 2016). In addition, REDD1 is well known to suppress mammalian target of rapamycin (mTOR) by inhibiting tuberous sclerosis complex (TSC) 1/2 (Brugarolas et al. 2004). Thus, we transfected cells with the dominant-negative mutant form of AMPK (DN-AMPK). But, the inhibitory effect of REDD1 on the fibrogenic gene expression was not affected (Fig. 13D). TGF-β, a profibrotic cytokine, activates mammalian target of rapamycin complex-1 (mTORC1) (Rozen-Zvi et al. 2013). P70S6K, the downstream signal transduction molecule of mTORC1, is essential for cell differentiation and growth as a key regulator of protein synthesis (Brown et al. 1994). Thus, p70s6K may affects HSC activation or fibrogenic gene induction. We transfected cells with constitutively active mutant form of p70s6K (CA-S6K) and measured since REDD1 is a negative regulator of mTORC1. However, it did not affect the inhibitory effect of REDD1 (Fig. 13E).

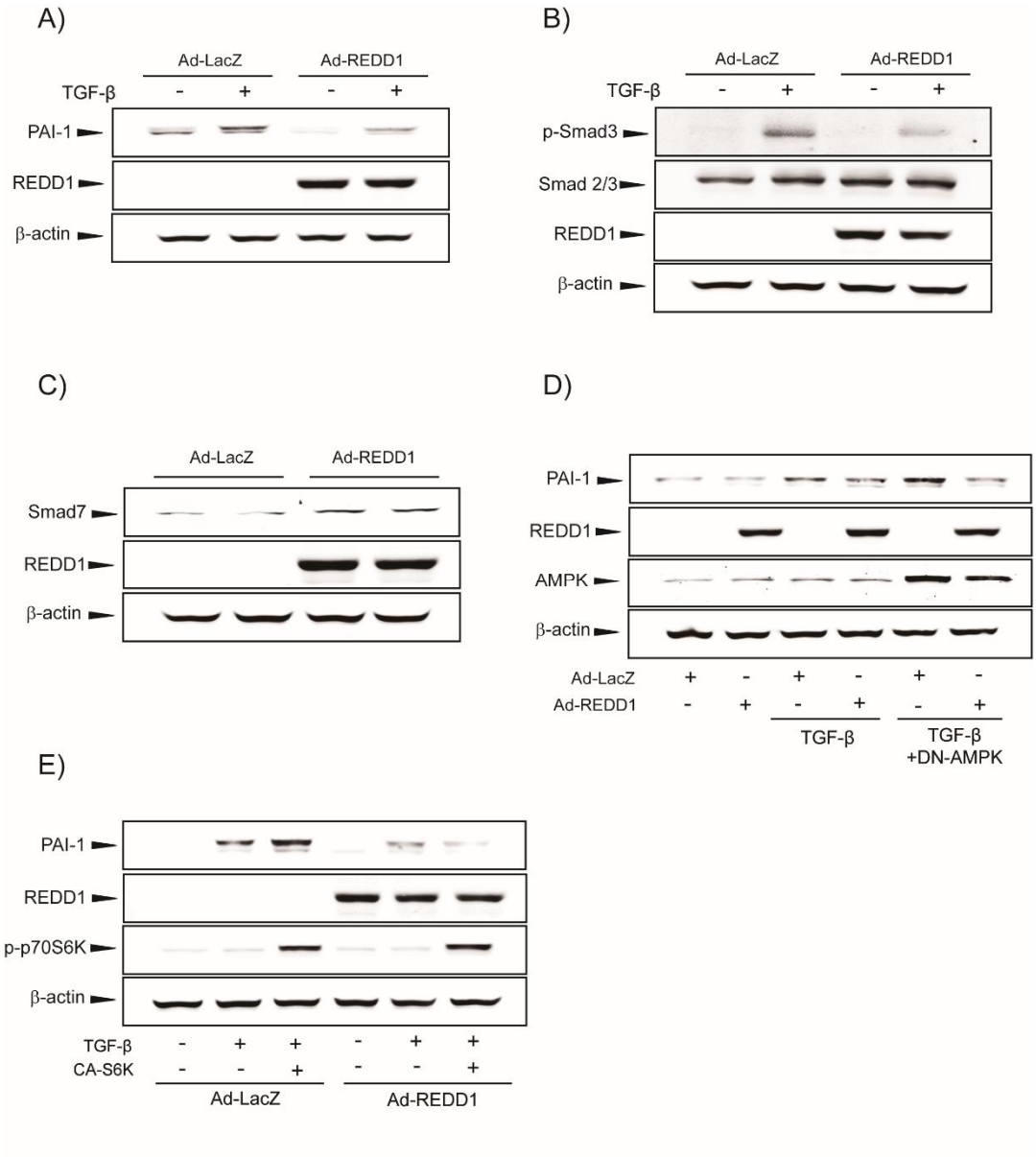

Figure 13. Inhibition of Smad signaling by REDD1

(A) LX-2 cells were infected with adenovirus expressing MOCK or REDD1. Then, TGF-β (1 ng/ml) were treated for 3 h. PAI-1 or REDD1 protein levels were determined by immunoblotting. (B) After overexpression of REDD1 using adenovirus, cells were treated with TGF-β for 30 m. Phosphorylation of Smad3 was measured by immunoblot analysis. (C) LX-2 cells were infected as described in (A) and treated with TGF-β (1 ng/mL) for 3 h. Smad7 protein level was determined by immunoblotting. (D) The role of AMPK in REDD1-mediated PAI-1 inhibition. LX-2 cells were infected with adenovirus expressing MOCK or REDD1. Then, we transfected cells with DN-AMPK and treated with TGF-β for 6 h. Protein levels were determined by immunoblotting. (E) The role of CA-S6K in REDD1-mediated PAI-1 inhibition. LX-2 cells were infected with adenovirus expressing MOCK or REDD1. Then, we transfected cells with CA-S6K and treated with TGF-β for 6 h. Protein levels were assessed by immunoblotting.

6. Protective effect of REDD1 against CCl_4-induced liver injury

To examine the effect of REDD1 on liver injury, we infected mice with a recombinant adenovirus expressing LacZ (Ad-LacZ) or REDD1 (Ad-REDD1). Adenovirus infection causes expression of exogenous gene especially in the liver (Fig. 14A). 48 h after viral infection, CCl_4 was intraperitoneally administered twice a week for 2 weeks. CCl_4 administration is the most commonly used method to induce liver fibrosis. Blood biochemical analysis showed that serum alanine aminotransferase (ALT) and aspartate aminotransferase (AST) levels were significantly increased by CCl_4 administration in mice. However, infection with adenovirus expressing REDD1 significantly inhibited the elevation of serum ALT and AST (Fig. 14A). Next, we conducted histopathological staining to investigate the extent of liver damage. In hematoxylin and eosin (H&E)-stained liver tissues, vehicle-treated Ad-LacZ or REDD1 mice were not observed any pathological changes. However, CCl_4 treatment increased focal hepatocellular necrosis, acute cellular swelling (ballooning), eosinophilic condensation, deposit of lipid droplets (fatty changes), and inflammatory cell infiltrations in Ad-LacZ-infected mice. On the other hand, Ad-REDD1 injected mice were significantly inhibited CCl_4-induced liver injury (Fig. 14B). CCl_4 treatments increased collagen deposition in Ad-LacZ-infected mice, and these effects were alleviated in Ad-REDD1-injected mice (Fig. 14C). Moreover, the number of α-SMA (HSC activation marker)-positive cells increased by CCl_4 was reduced by Ad-REDD1 administration (Fig. 14D).

Next, we measured GSH contents in CCl_4- or vehicle-treated mice liver tissues. GSH level was reduced by CCl_4 in Ad-LacZ infected mice. However, the decreased GSH contents was significantly restored by Ad-REDD1 (Fig. 15A). In addition, we examined the formation of malondialdehyde (MDA), the final product of lipid peroxidation. Treatment of CCl_4 was increased the MDA contents in Ad-LacZ-injected mice, but this effect was markedly inhibited

by Ad-REDD1 administration. (Fig. 15B). We next assessed fibrosis marker in the liver by immunoblotting. The fibrosis markers, such as α-SMA, PAI-1 or collagen were increased by CCl_4 treatment in Ad-LacZ-injected mice (Fig. 15C). These findings suggest that REDD1 protects against liver fibrosis induced by CCl_4.

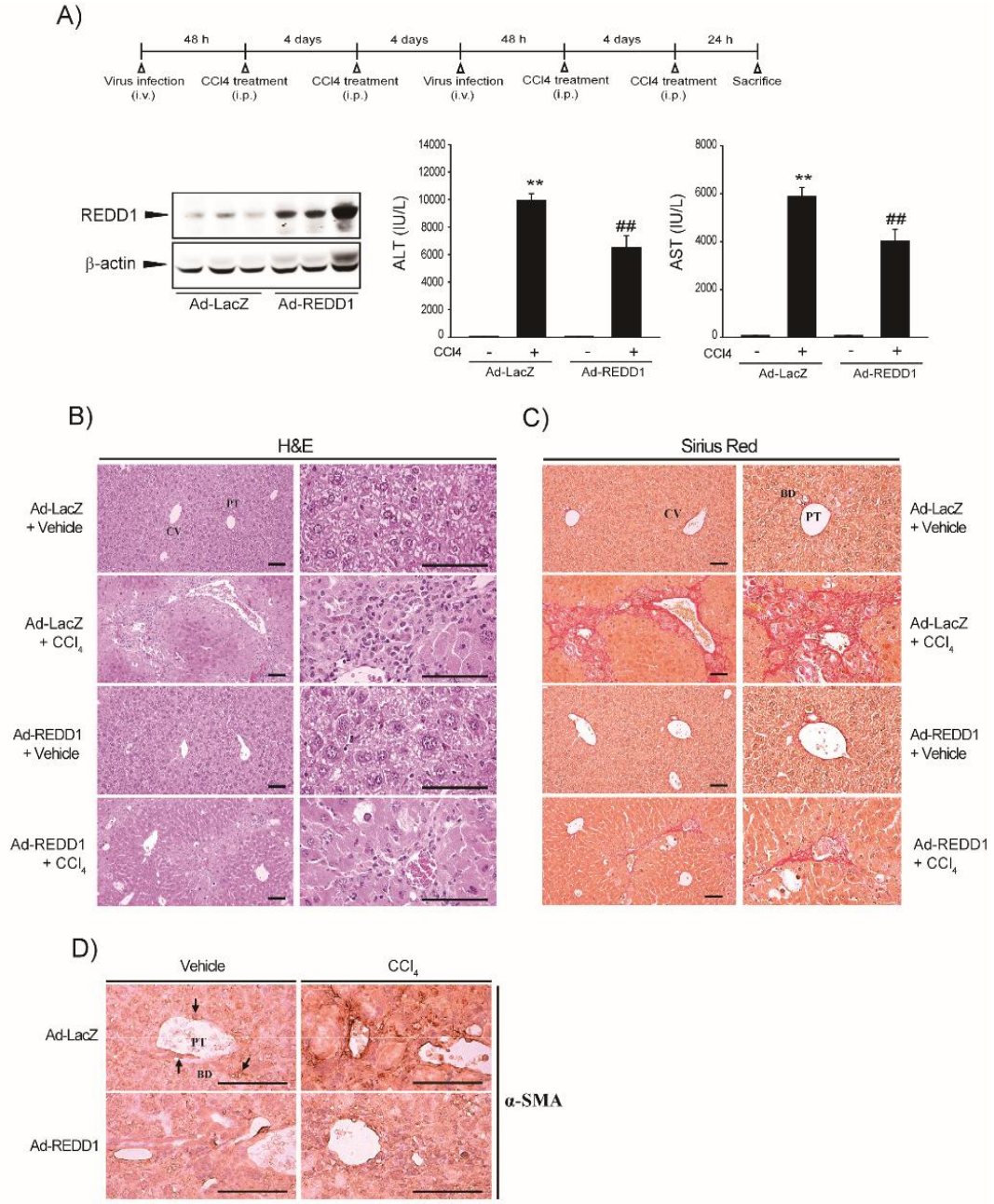

Figure 14. Inhibition of CCl_4-induced liver fibrosis by Ad-REDD1

(A) CCl_4 administration schedule to induce liver fibrosis (upper). REDD1 expression was confirmed in liver homogenates infected with adenovirus LacZ (Ad-LacZ) or REDD1 (Ad-REDD1) (lower left). ALT and AST activities were measured by commercial kits. Data represent means ± S.E. of five replicates (significant compared with vehicle-treated Ad-LacZ mice, **$p<0.01$; significant compared with CCl_4-treated Ad-LacZ mice, $^{\#\#}p<0.01$) (lower right) (B and C) Representative histological image of the liver. Samples were stained with Hematoxylin and eosin (H&E) or Sirius Red (scale bar = 120 μm) (D) α-SMA immunohistochemistry in liver tissues of mice injected with vehicle or CCl_4 (scale bar = 120 μm). CV, central vein; PT, portal triad; BD, bile duct.

Table 3. Histomorphometrical analysis of hepatic tissues, taken form vehicle or CCl_4-treated mice

Groups	Ad-LacZ		Ad-REDD1	
Index (Unit)	Vehicle	CCl4	Vehicle	CCl4
Hepatic Staging Scores (Max = 6)*	0.25±0.46	4.13±0.83[a]	0.25±0.46[b]	2.00±0.93[abc]
DE regions (%/mm^2)	3.02±2.69	64.09±12.05[d]	3.04±2.46[e]	29.29±11.19[def]
DE hepatocytes (cells/1000 hepatocytes)†	26.00±25.41	589.00±126.57[d]	26.75±24.07[e]	232.25±86.89[def]
Inflammatory cells (cells/1000 hepatocytes)	21.75±15.17	414.50±109.30[d]	21.00±12.51[e]	167.00±74.91[def]
SR stained collagen occupied regions (%/mm^2)	1.27±0.93	29.78±10.30[d]	1.25±0.99[e]	12.18±6.32[def]
Mean α-SMA immunoreactive cell numbers	12.75±8.55	225.75±109.56[d]	12.25±8.91[e]	64.25±22.81[def]

Values are expressed as mean ± SD of 8 histological fields

CCl_4 = Carbon tetrachloride; Ad-LacZ = Recombinant adenovirus particles (1×10^8 pfu) expressing LacZ; REDD1 = The protein regulated in development and DNA damage responses1; Ad-REDD1 = Recombinant adenovirus particles (1×10^8 pfu) expressing REDD1; DE = Degenerative; SD = Standard deviation; H&E = Hematoxylin and eosin; SR = Sirius red; LSD = Least-significant differences multi-comparison; MW = Mann-Whitney U

CCl_4 was intraperitoneal injection, two times/week for two weeks, at dose level of 0.5 mg/kg

Test articles were intravenously treated via a tail vein 48 h prior to CCl_4 treatment

* Details of Hepatic Staging Scores

No fibrosis	0
Fibrous expansion of some portal areas, with or without short fibrous septa	1
Fibrous expansion of most portal areas, with or without short fibrous septa	2
Fibrous expansion of most portal areas with occasional P-P bridging	3
Fibrous expansion of portal areas with marked bridging P-P as well as P-C	4
Marked bridging (P-P and/or P-C) with occasional nodules (incomplete cirrhosis)	5
Cirrhosis, probable or definite	6

P-P = Portal to portal
P-C = Portal to central
Possible maximum total scores = 6
Modified from the method described by Ishak et al. 1995

† Hepatocytes showing any degenerative changes including acute cellular swelling (ballooning), focal necrosis, eosinophilic condensation, and lipid droplet accumulations (fatty changes) were regarded as "Degenerative hepatocytes" under H&E stain

[a] $p<0.01$ as compared to those of Ad-LacZ control by LSD test

[b] $p<0.01$ as compared to those of Ad-LacZ CCl4 by LSD test

[c] $p<0.01$ as compared to those of Ad-REDD1 control by LSD test

[d] $p<0.01$ as compared to those of Ad-LacZ control by MW test

[e] $p<0.01$ as compared to those of Ad-LacZ CCl4 by MW test

[f] $p<0.01$ as compared to those of Ad-REDD1 control by MW test

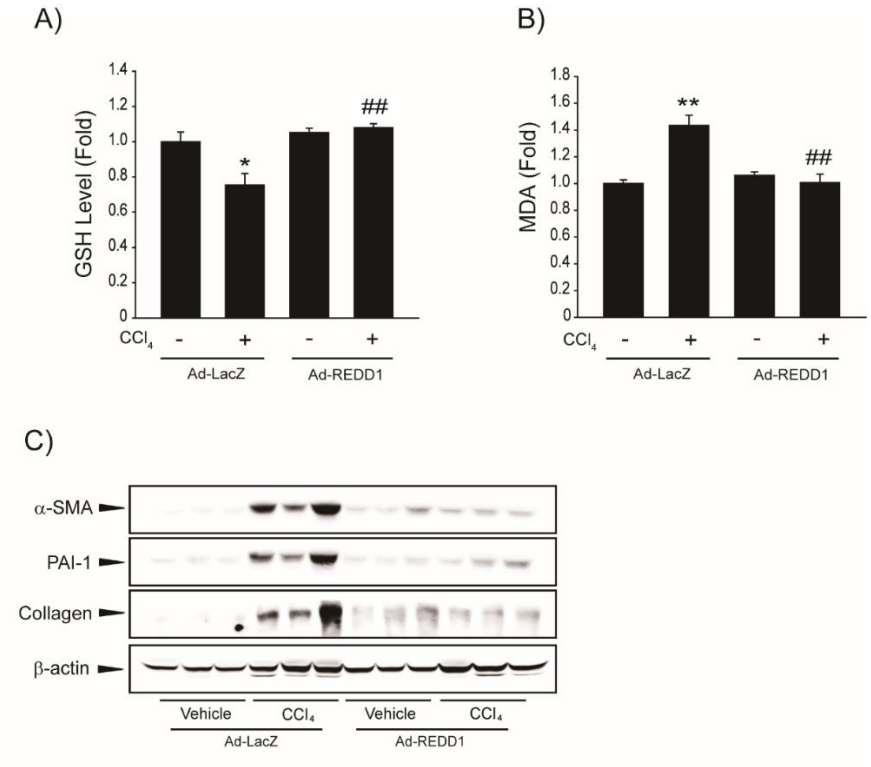

Figure 15. Inhibition of CCl_4 induced fibrotic liver damage by Ad-REDD1

(A) GSH contents were measured in mice liver homogenates. Data represent means ± S.E. of five replicates (significant compared with vehicle-treated Ad-LacZ mice, **p<0.01; significant compared with CCl_4-treated Ad-LacZ mice, ##p<0.01) (B) MDA quantitation by TBARS assay in liver homogenates. Data represent the mean ± S.E. of five replicates; significant compared with vehicle-treated Ad-LacZ mice, **p<0.01; significant compared with CCl4-treated Ad-LacZ mice, ##p<0.01 (C) Fibrosis marker protein, such as a-SMA, PAI-1 and collagen, levels were assessed by immunoblotting.

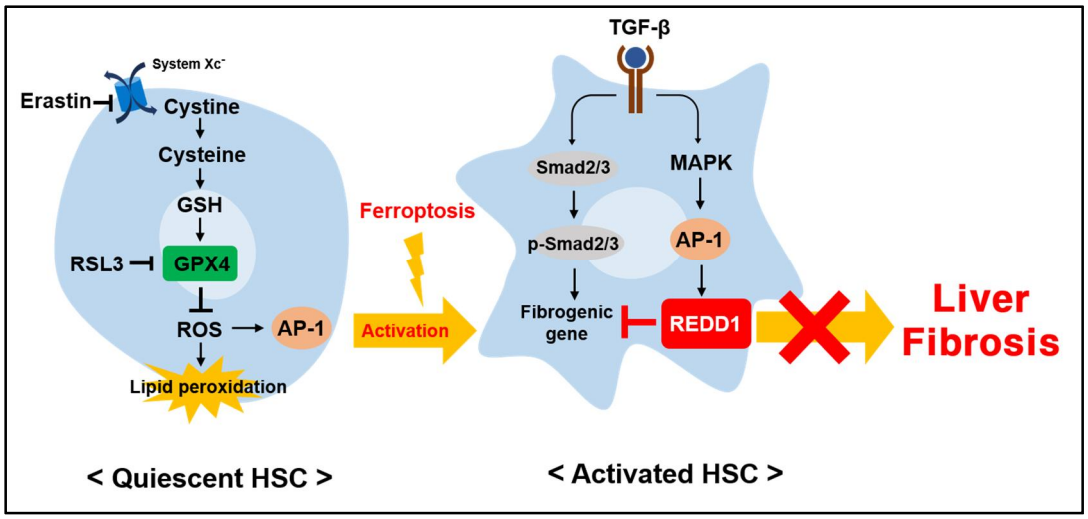

Figure 16. Role of REDD1 in ferroptosis-mediated liver fibrosis

Schematic diagram illustrating the mechanism by which REDD1 inhibited ferroptosis-mediated liver fibrosis.

IV. DISCUSSION

In the current study, we determined whether ferroptosis affects HSC activation and further investigated the role of REDD1 induction in HSC activation. Here, we found the following: (1) ferroptosis contributes to HSC activation; (2) Ferroptosis induced by chronic iron deposition causes liver fibrosis *in vivo*; (3) REDD1 expression is upregulated during HSC activation and (4) Elevated REDD1 has anti-fibrotic effect in liver. To the best of our knowledge, this is the first report of the role of REDD1 in ferroptosis-mediated liver fibrosis.

Ferroptosis was first described as iron-dependent cell death, and not depend on other metals (Dixon et al. 2012). Ferroptosis is also due to occurrence of lethal lipid peroxidation (Stockwell et al. 2017). It is also genetically distinct from other form of cell death, such as apoptosis, necroptosis, and autophagy (Dixon et al. 2012). Iron overload contributes to human pathologies in various tissues including the liver (Bogdan et al. 2016). It has been reported that ferroptosis occured in the liver of high iron diet feeding mice and knockout mice that develop-iron overload (Wang et al. 2017). It has also been demonstrated that ferroptosis was induced in liver injury models such as acetaminophen overdose intake (Lorincz et al. 2015) and ischemia/reperfusion (Friedmann Angeli et al. 2014). In addition, we recently reported that ferroptosis occured in mice liver administered with phenylhydrazine (PHZ), a well-established iron overload inducing model (Comporti et al. 1996, Park, 2019). These findings suggest that ferroptosis induced by iron deposition causes liver injury.

Recently, we suggested Sestrin2 as a therapeutic target for ferroptosis-mediated parenchymal hepatocyte damage (Park et al. 2019). However, the role of ferroptosis in non-parenchymal liver cells is not examined yet. In this study, we first identified the effects of ferroptosis-inducers in

HSCs. Ferroptosis inducers such as RSL3 or erastin caused cell death in HSC, and cell viabilities were specifically recovered by ferrostatin or DFO (Fig. 1B). In addition, we observed the changes of ferroptosis markers, such as GPX4 expression, GSH contents, lipid ROS and iron transport genes (Fig. 2). These results suggest that ferroptosis occurs in HSCs as well as hepatocytes. Stimulation of HSCs with ferroptosis inducers such as, RSL3 and Fe-NTA also increased PAI-1, an HSC activation marker (Fig. 2F and 3A). However, increased PAI-1 was inhibited by ferrostatin-1 treatment, which indicates that ferroptosis contribute to HSC activation (Fig. 3C).

Signaling pathways by typical HSC activation stimuli are divided into canonical and non-canonical pathway (Derynck and Zhang 2003). Previously, we reported that inhibition of c-JUN-dependent AP-1 activation was associated with anti-fibrotic effects in HSCs (Kim et al. 2020). In addition, AP-1 was increased in activated HSCs and regulates ECM remodeling-related genes (Li et al. 2008). Therefore, we initially observed the effect of RSL3 on AP-1 activation. Phosphorylation of c-JUN and AP-1 luciferase activity was increased in HSCs by TGF-β (Fig. 4A and B). Also, c-JUN phosphorylation was inhibited by treatment of ferrostatin-1 (Fig. 4C and D). However, phosphorylation of Smad2 or Smad3 were not affected. In the signaling pathway of TGF-β, the most well-studied profibrotic cytokines, the Smad activation is well known as a key mediator (Inagaki and Okazaki 2007). These results indicate that the AP-1 signaling pathway is crucial for RSL3-mediated HSC activation.

Based on the results obtained so far, we determined the effect of ferroptosis on HSC activation. Ferroptosis inducers contributed to HSC activation by causing cell damage through GSH depletion, GPX4 inhibition, and increased production of ROS and lipid ROS. However, to clarify the correlation between HSC activation and ferroptosis, we conducted experiments whether ferroptosis occurs during HSC activation. We first confirmed that GPX4 protein was down-regulated in activated HSCs (Fig. 5A). In addition, decreased GPX4 expression and increased

ROS production were observed by TGF-β treatment (Fig. 5B and D). The decreased GPX4 expression was restored by ferrostatin treatment (Fig. 5C). These results indicate that ferroptotic condition is driven during HSC activation.

There is no animal model for the ferroptosis-mediated liver fibrosis. Thus, we have tried to establish animal model mimic ferroptosis-mediated liver fibrosis. Long-term treatment with iron dextran results in excess iron accumulation in liver, resulting in liver damage (Zhang et al. 2013). Therefore iron dextran-induced liver injury in mice was adopted to support our *in vitro* findings that ferroptosis contribute to HSC activation. Mouse serum ALT and AST levels were significantly increased by iron dextran administration. In addition, histological data showed that focal hepatocellular necrosis, acute cellular swelling (ballooning), eosinophilic condensation and inflammatory cell infiltrations were increased in the iron dextran-administered group (Fig. 6). Changes in ferroptosis markers, such as lipid peroxidation, GSH depletion, GPX4 expression and iron accumulation were observed in iron dextran administered mouse liver (Fig. 7). Furthermore, increases α-SMA and PAI-1, known as HSC activation markers, were observed through immunoblotting and IHC staining. Collagen accumulation was also observed using Sirius Red staining (Fig. 8). Although the results obtained from ferroptosis animal models provide evidence that ferroptosis contribute to progression of liver fibrosis, this study has limitation. GSH depletion and GPX4 inhibition were observed in mice treated with iron dextran for 8-12 weeks, but increased inversely in mice treated for 16-20 weeks. Moreover, in a condition of the current histopathological analysis, obvious hepatic fibrosis was demonstrated from 20 weeks after iron dextran injection. This phenomenon may be due to a compensatory response for survival against chronic damage caused by prolonged administration of iron dextran. More specific mechanism study should be required for resolving this limitation. Our results may provide the assistance in understanding the pathophysiological role of ferroptosis in the liver.

We previously reported that REDD1 antagonized oxidative stress-mediated hepatocyte injury. Here, we found that REDD1 is upregulated in activated HSCs and TGF-β treated LX-2 cells. REDD1 expression is mainly regulated by AP-1 and inhibited fibrogenesis in HSC and mouse liver. These findings suggest that REDD1 induction in HSCs ameliorates liver fibrosis. In our recent study showed that induction of REDD1 prevents ROS generation and cell death in hepatocytes (Cho et al. 2018). However, the pathophysiological role and regulatory mechanism of REDD1 in hepatic stellate cells, including hepatocytes, has not been investigated and further studies are necessary to reveal this.

In our results, TGF-β-mediated REDD1 induction is transcriptionally regulated and that c-JUN is an essential molecule for TGF-β dependent REDD1 gene expression. TGF-β is produced by exogenous ROS in HSC and vice versa (Urtasun et al. 2008). Oxidative stress leads to ROS-mediated cell damage (Emerit and Michelson 1982). In HSCs, ROS is major cause of activation, which crucial for fibrotic response following liver injury (Poli 2000). We previously reported that REDD1-dependent protective effect against oxidative stress is mediated through AP-1 (Cho et al. 2018). In addition, AP-1 is well known as major redox sensitive transcription factors (Korashy and El-Kadi 2008). So, we confirmed that c-JUN phosphorylation and AP-1 luciferase activity was increased by TGF-β treatment (Fig. 11E and F). Moreover, we observed that REDD1 protein level and luciferase activity were increased by c-JUN expressing plasmid transfection (Fig. 11C and D). However, REDD1 expression was not altered by Smad3 expressing plasmid transfection in LX-2 cells. (Fig. 11A and B). TGF-β signals through receptors, composed of type I and II heterodimers and initiate downstream signaling via phosphorylation of Smad proteins (Massague 2012).

TGF-β dominantly signals through Smad, but it can also affect via Smad-independent pathways, such as MAPK (Zhang 2009). Our results obtained from using chemical inhibitors of

MAPK showed REDD1 induction by TGF-β was antagonized by p38 specific chemical inhibitor (Fig. 11G). These results indicate that TGF-β-dependent p38 MAPK phosphorylation contributes to the induction of REDD1 in HSCs.

To reveal the specific AP-1 binding region by TGF-β in human REDD1 promoter, reporter gene analysis was performed using serially deleted REDD1 promoter constructs as previously described (Cho et al. 2018) (Fig. 12A). Then, we found the sequence deletion between −716 to −587 bp significantly inhibited transactivation of REDD1 by TGF-β (Fig. 12B). These results suggest that putative AP-1 binding region from −716 to −587 bp of human REDD1 promoter is critical region to transactivate REDD1.

To determine the functional role of REDD1, we assessed the effect of REDD1 on TGF-β-mediated fibrogenic gene induction and Smad activation. As a result, REDD1 overexpression attenuated Smad3 phosphorylation and PAI-1 expression (Fig. 13A and B). In addition, reduction of Smad3 activity by overexpression of REDD1 was accompanied by increased Smad7 expression (inhibitory factor) (Fig. 13C). To investigate the concise mechanisms mediating the anti-fibrotic effect of REDD1, we evaluated using mutant form of AMPK or S6K. AMPK and S6K have been reported to involved in mTOR complex-mediated fibrogenic gene expression (Yang et al. 2018, Jiang, 2017). Albeit abolished AMPK activity or continuously induced activity of S6K did not affect inhibitory effect of REDD1 (Fig. 13D and E). Identification of unrevealed factors that mediate the inhibitory effect of REDD1 should be studied through further study.

The results obtained from ferroptosis-mediated fibrosis animal model suggest that induction of REDD1 can be a promising strategy of treating or preventing liver fibrosis. However, we could not exclude the possibility that protective effect of Ad-REDD1 was probably due to the combined effects of hepatocytes and HSCs, because the adenovirus is not HSC-specific delivery system. Thus, we are now developed HSCs specific gene delivery system and demonstrate role of

REDD1 in hepatic fibrosis animal models.

Collectively, our results provide insight into the ferroptosis-mediated fibrogenesis in liver and can be of assistance in understanding the pathophysiological role of REDD1 gene in liver fibrosis (Fig. 16).

REFERENCES

Andrews and Schmidt (2007). "Iron homeostasis." Annu Rev Physiol 69: 69-85.

Arpino, Brock and Gill (2015). "The role of TIMPs in regulation of extracellular matrix proteolysis." Matrix Biol 44-46: 247-254.

Bai, Wang, Zhao, Zhu, Wang and Sun (2017). "Haloperidol, a sigma receptor 1 antagonist, promotes ferroptosis in hepatocellular carcinoma cells." Biochem Biophys Res Commun 491(4): 919-925.

Bochkov, Oskolkova, Birukov, Levonen, Binder and Stockl (2010). "Generation and biological activities of oxidized phospholipids." Antioxid Redox Signal 12(8): 1009-1059.

Bogdan, Miyazawa, Hashimoto and Tsuji (2016). "Regulators of Iron Homeostasis: New Players in Metabolism, Cell Death, and Disease." Trends Biochem Sci 41(3): 274-286.

Brigelius-Flohe and Maiorino (2013). "Glutathione peroxidases." Biochim Biophys Acta 1830(5): 3289-3303.

Brown, Albers, Shin, Ichikawa, Keith, Lane and Schreiber (1994). "A mammalian protein targeted by G1-arresting rapamycin-receptor complex." Nature 369(6483): 756-758.

Brugarolas, Lei, Hurley, Manning, Reiling, Hafen, Witters, Ellisen and Kaelin (2004).

"Regulation of mTOR function in response to hypoxia by REDD1 and the TSC1/TSC2 tumor suppressor complex." Genes Dev 18(23): 2893-2904.

Chang, Chiang, Chen, Yu, Chou and Chang (2018). "Heme oxygenase-1 mediates BAY 11-7085 induced ferroptosis." Cancer Lett 416: 124-137.

Cho, Kim, Han, Kim, Anderson, Lee, Lee, Hwang and Kim (2010). "E-cadherin antagonizes transforming growth factor beta1 gene induction in hepatic stellate cells by inhibiting RhoA-dependent Smad3 phosphorylation." Hepatology 52(6): 2053-2064.

Cho, Kim, Yang, Kim, Park, Kim, Kim, Cho and Ki (2018). "Induction of REDD1 via AP-1 prevents oxidative stress-mediated injury in hepatocytes." Free Radic Biol Med 124: 221-231.

Comporti, Signorini, Sugherini, Pompella, Ciccoli and Ferrali (1996). Hepatic Iron Overload Induced by Phenylhydrazine: Release of Iron in a Free Form and DNA Damage. New Trends in Hepatology: The Proceedings of the Annual Meeting of the Italian National Programme on Liver Cirrhosis and Viral Hepatitis, San Miniato (Pisa), Italy, 7–9 January, 1996. Gentilini and Dianzani. Dordrecht, Springer Netherlands: 56-64.

Derynck and Zhang (2003). "Smad-dependent and Smad-independent pathways in TGF-beta family signalling." Nature 425(6958): 577-584.

Distefano, Martin, Cordoba, Bellido, D'Ippolito, Colman, Soto, Roldan, Bartoli, Zabaleta, Fiol, Stockwell, Dixon and Pagnussat (2017). "Heat stress induces ferroptosis-like cell death in

plants." J Cell Biol 216(2): 463-476.

Dixon, Lemberg, Lamprecht, Skouta, Zaitsev, Gleason, Patel, Bauer, Cantley, Yang, Morrison and Stockwell (2012). "Ferroptosis: an iron-dependent form of nonapoptotic cell death." Cell 149(5): 1060-1072.

Dixon and Stockwell (2014). "The role of iron and reactive oxygen species in cell death." Nat Chem Biol 10(1): 9-17.

Dixon, Winter, Musavi, Lee, Snijder, Rebsamen, Superti-Furga and Stockwell (2015). "Human Haploid Cell Genetics Reveals Roles for Lipid Metabolism Genes in Nonapoptotic Cell Death." ACS Chem Biol 10(7): 1604-1609.

Dolma, Lessnick, Hahn and Stockwell (2003). "Identification of genotype-selective antitumor agents using synthetic lethal chemical screening in engineered human tumor cells." Cancer Cell 3(3): 285-296.

Emerit and Michelson (1982). "[Free radicals in medicine and biology]." Sem Hop 58(45): 2670-2675.

Fatokun, Dawson and Dawson (2014). "Parthanatos: mitochondrial-linked mechanisms and therapeutic opportunities." Br J Pharmacol 171(8): 2000-2016.

Friedmann Angeli, Schneider, Proneth, Tyurina, Tyurin, Hammond, Herbach, Aichler, Walch,

Eggenhofer, Basavarajappa, Radmark, Kobayashi, Seibt, Beck, Neff, Esposito, Wanke, Forster, Yefremova, Heinrichmeyer, Bornkamm, Geissler, Thomas, Stockwell, O'Donnell, Kagan, Schick and Conrad (2014). "Inactivation of the ferroptosis regulator Gpx4 triggers acute renal failure in mice." Nat Cell Biol 16(12): 1180-1191.

Gangnuss, Cowin, Daehn, Hatzirodos, Rothnagel, Varelias and Rayner (2004). "Regulation of MAPK activation, AP-1 transcription factor expression and keratinocyte differentiation in wounded fetal skin." J Invest Dermatol 122(3): 791-804.

Gaschler, Andia, Liu, Csuka, Hurlocker, Vaiana, Heindel, Zuckerman, Bos, Reznik, Ye, Tyurina, Lin, Shchepinov, Chan, Peguero-Pereira, Fomich, Daniels, Bekish, Shmanai, Kagan, Mahal, Woerpel and Stockwell (2018). "FINO2 initiates ferroptosis through GPX4 inactivation and iron oxidation." Nat Chem Biol 14(5): 507-515.

Gui, Sun, Shimokado and Muragaki (2012). "The Roles of Mitogen-Activated Protein Kinase Pathways in TGF-beta-Induced Epithelial-Mesenchymal Transition." J Signal Transduct 2012: 289243.

Hassannia, Vandenabeele and Vanden Berghe (2019). "Targeting Ferroptosis to Iron Out Cancer." Cancer Cell 35(6): 830-849.

Hayano, Yang, Corn, Pagano and Stockwell (2016). "Loss of cysteinyl-tRNA synthetase (CARS) induces the transsulfuration pathway and inhibits ferroptosis induced by cystine deprivation." Cell Death Differ 23(2): 270-278.

Hentze, Muckenthaler, Galy and Camaschella (2010). "Two to tango: regulation of Mammalian iron metabolism." Cell 142(1): 24-38.

Horak, Crawford, Vadysirisack, Nash, DeYoung, Sgroi and Ellisen (2010). "Negative feedback control of HIF-1 through REDD1-regulated ROS suppresses tumorigenesis." Proc Natl Acad Sci U S A 107(10): 4675-4680.

Hou, Xie, Song, Sun, Lotze, Zeh, Kang and Tang (2016). "Autophagy promotes ferroptosis by degradation of ferritin." Autophagy 12(8): 1425-1428.

Inagaki and Okazaki (2007). "Emerging insights into Transforming growth factor beta Smad signal in hepatic fibrogenesis." Gut 56(2): 284-292.

Jin, Yang, Shin, Seo, Shin, Cho and Ki (2013). "Resveratrol inhibits LXRalpha-dependent hepatic lipogenesis through novel antioxidant Sestrin2 gene induction." Toxicol Appl Pharmacol 271(1): 95-105.

Kim, Han, Kim, Cho, Kim, Koo, Lee, Lim, Kang, Kim, Hwang, Ki and Kim (2018). "Galpha12 overexpression induced by miR-16 dysregulation contributes to liver fibrosis by promoting autophagy in hepatic stellate cells." J Hepatol 68(3): 493-504.

Kim, Kim, Yang, Cho, Kim, Park, Ahn, Lee, Yang, Lim, Kang and Ki (2020). "Induction of E6AP by microRNA-302c dysregulation inhibits TGF-beta-dependent fibrogenesis in hepatic stellate cells." Sci Rep 10(1): 444.

Kim, Yang, Shin, Cho and Ki (2015). "Sestrin2: A Promising Therapeutic Target for Liver Diseases." Biol Pharm Bull 38(7): 966-970.

Knittel, Fellmer and Ramadori (1996). "Gene expression and regulation of plasminogen activator inhibitor type I in hepatic stellate cells of rat liver." Gastroenterology 111(3): 745-754.

Knudsen, Gopal and Singal (2014). "The changing landscape of hepatocellular carcinoma: etiology, genetics, and therapy." Am J Pathol 184(3): 574-583.

Korashy and El-Kadi (2008). "The role of redox-sensitive transcription factors NF-kappaB and AP-1 in the modulation of the Cyp1a1 gene by mercury, lead, and copper." Free Radic Biol Med 44(5): 795-806.

Li, Liao, Ping, Xu and Wang (2008). "Molecular mechanism of hepatic stellate cell activation and antifibrotic therapeutic strategies." J Gastroenterol 43(6): 419-428.

Liu, Baker, Bhatia, Zhu and Baker (2016). "Pathogenesis of nonalcoholic steatohepatitis." Cell Mol Life Sci 73(10): 1969-1987.

Llovet, Ricci, Mazzaferro, Hilgard, Gane, Blanc, de Oliveira, Santoro, Raoul, Forner, Schwartz, Porta, Zeuzem, Bolondi, Greten, Galle, Seitz, Borbath, Haussinger, Giannaris, Shan, Moscovici, Voliotis, Bruix and Group (2008). "Sorafenib in advanced hepatocellular carcinoma." N Engl J Med 359(4): 378-390.

Lorincz, Jemnitz, Kardon, Mandl and Szarka (2015). "Ferroptosis is Involved in Acetaminophen Induced Cell Death." Pathol Oncol Res 21(4): 1115-1121.

Louandre, Ezzoukhry, Godin, Barbare, Maziere, Chauffert and Galmiche (2013). "Iron-dependent cell death of hepatocellular carcinoma cells exposed to sorafenib." Int J Cancer 133(7): 1732-1742.

Louandre, Marcq, Bouhlal, Lachaier, Godin, Saidak, Francois, Chatelain, Debuysscher, Barbare, Chauffert and Galmiche (2015). "The retinoblastoma (Rb) protein regulates ferroptosis induced by sorafenib in human hepatocellular carcinoma cells." Cancer Lett 356(2 Pt B): 971-977.

Luo, Han, Chin and Linn (1994). "Three chemically distinct types of oxidants formed by iron-mediated Fenton reactions in the presence of DNA." Proc Natl Acad Sci U S A 91(26): 12438-12442.

Massague (2012). "TGFbeta signalling in context." Nat Rev Mol Cell Biol 13(10): 616-630.

McBean (2012). "The transsulfuration pathway: a source of cysteine for glutathione in astrocytes." Amino Acids 42(1): 199-205.

Molitoris, McColl, Swerdlow, Matsuyama, Lam, Finkel, Matsuyama and Distelhorst (2011). "Glucocorticoid elevation of dexamethasone-induced gene 2 (Dig2/RTP801/REDD1) protein mediates autophagy in lymphocytes." J Biol Chem 286(34): 30181-30189.

Moosmann and Behl (2004). "Selenoproteins, cholesterol-lowering drugs, and the consequences:

revisiting of the mevalonate pathway." Trends Cardiovasc Med 14(7): 273-281.

Paik, Kim, Aoyama, De Minicis, Bataller and Brenner (2014). "Role of NADPH oxidases in liver fibrosis." Antioxid Redox Signal 20(17): 2854-2872.

Park, Cho, Kim, Yang, Kim, Jeong, Yang, Han, Ku, Cho and Ki (2019). "Protective effect of sestrin2 against iron overload and ferroptosis-induced liver injury." Toxicol Appl Pharmacol 379: 114665.

Parola and Robino (2001). "Oxidative stress-related molecules and liver fibrosis." J Hepatol 35(2): 297-306.

Poli (2000). "Pathogenesis of liver fibrosis: role of oxidative stress." Mol Aspects Med 21(3): 49-98.

Qi, Kim, Zhou, Lim and Kim (2020). "Ferroptosis Affects the Progression of Nonalcoholic Steatohepatitis via the Modulation of Lipid Peroxidation-Mediated Cell Death in Mice." Am J Pathol 190(1): 68-81.

Qi, Li, Xia, Dai, Zhang, Wu and Xu (2019). "LncRNA GABPB1-AS1 and GABPB1 regulate oxidative stress during erastin-induced ferroptosis in HepG2 hepatocellular carcinoma cells." Sci Rep 9(1): 16185.

Qiao, Dennis, Song, Vadysirisack, Salunke, Nash, Yang, Liesa, Yoshioka, Matsuzawa, Shirihai,

Lee, Reed and Ellisen (2015). "A REDD1/TXNIP pro-oxidant complex regulates ATG4B activity to control stress-induced autophagy and sustain exercise capacity." Nat Commun 6: 7014.

Rozen-Zvi, Hayashida, Hubchak, Hanna, Platanias and Schnaper (2013). "TGF-beta/Smad3 activates mammalian target of rapamycin complex-1 to promote collagen production by increasing HIF-1alpha expression." Am J Physiol Renal Physiol 305(4): F485-494.

Sato, Tamba, Ishii and Bannai (1999). "Cloning and expression of a plasma membrane cystine/glutamate exchange transporter composed of two distinct proteins." J Biol Chem 274(17): 11455-11458.

Shang, Luo, Yao, Wang, Yuan and Yang (2020). "Ceruloplasmin suppresses ferroptosis by regulating iron homeostasis in hepatocellular carcinoma cells." Cell Signal 72: 109633.

Shimada, Skouta, Kaplan, Yang, Hayano, Dixon, Brown, Valenzuela, Wolpaw and Stockwell (2016). "Global survey of cell death mechanisms reveals metabolic regulation of ferroptosis." Nat Chem Biol 12(7): 497-503.

Shin, Jin, Cho and Ki (2012). "Nrf2-ARE pathway regulates induction of Sestrin-2 expression." Free Radic Biol Med 53(4): 834-841.

Stockwell, Friedmann Angeli, Bayir, Bush, Conrad, Dixon, Fulda, Gascon, Hatzios, Kagan, Noel, Jiang, Linkermann, Murphy, Overholtzer, Oyagi, Pagnussat, Park, Ran, Rosenfeld, Salnikow, Tang, Torti, Torti, Toyokuni, Woerpel and Zhang (2017). "Ferroptosis: A Regulated Cell Death

Nexus Linking Metabolism, Redox Biology, and Disease." Cell 171(2): 273-285.

Sun, Niu, Chen, He, Chen, Kang and Tang (2016). "Metallothionein-1G facilitates sorafenib resistance through inhibition of ferroptosis." Hepatology 64(2): 488-500.

Sun, Ou, Chen, Niu, Chen, Kang and Tang (2016). "Activation of the p62-Keap1-NRF2 pathway protects against ferroptosis in hepatocellular carcinoma cells." Hepatology 63(1): 173-184.

Sutherland, Shankaranarayanan, Schewe and Nigam (2001). "Evidence for the presence of phospholipid hydroperoxide glutathione peroxidase in human platelets: implications for its involvement in the regulatory network of the 12-lipoxygenase pathway of arachidonic acid metabolism." Biochem J 353(Pt 1): 91-100.

Suttner and Dennery (1999). "Reversal of HO-1 related cytoprotection with increased expression is due to reactive iron." FASEB J 13(13): 1800-1809.

Svegliati Baroni, D'Ambrosio, Ferretti, Casini, Di Sario, Salzano, Ridolfi, Saccomanno, Jezequel and Benedetti (1998). "Fibrogenic effect of oxidative stress on rat hepatic stellate cells." Hepatology 27(3): 720-726.

Tsurusaki, Tsuchiya, Koumura, Nakasone, Sakamoto, Matsuoka, Imai, Yuet-Yin Kok, Okochi, Nakano, Miyajima and Tanaka (2019). "Hepatic ferroptosis plays an important role as the trigger for initiating inflammation in nonalcoholic steatohepatitis." Cell Death Dis 10(6): 449.

Urtasun, Conde de la Rosa and Nieto (2008). "Oxidative and nitrosative stress and fibrogenic response." Clin Liver Dis 12(4): 769-790, viii.

Verbon, Trapet, Stringlis, Kruijs, Bakker and Pieterse (2017). "Iron and Immunity." Annu Rev Phytopathol 55: 355-375.

Wang, An, Xie, Wu, Fang, Gao, Zhang, Li, Wang, Zhang, Li, Yang, Liu, Min and Wang (2017). "Characterization of ferroptosis in murine models of hemochromatosis." Hepatology 66(2): 449-465.

Wang, Chen, Shi, Jiao and Gong (2019). "Mechanism of glycyrrhizin on ferroptosis during acute liver failure by inhibiting oxidative stress." Mol Med Rep 20(5): 4081-4090.

Wang, Kubica, Ellisen, Jefferson and Kimball (2006). "Dexamethasone represses signaling through the mammalian target of rapamycin in muscle cells by enhancing expression of REDD1." J Biol Chem 281(51): 39128-39134.

Weiwer, Bittker, Lewis, Shimada, Yang, MacPherson, Dandapani, Palmer, Stockwell, Schreiber and Munoz (2012). "Development of small-molecule probes that selectively kill cells induced to express mutant RAS." Bioorg Med Chem Lett 22(4): 1822-1826.

Whalen, Rockey, Friedman and Boyer (1999). "Activation of rat hepatic stellate cells leads to loss of glutathione S-transferases and their enzymatic activity against products of oxidative stress." Hepatology 30(4): 927-933.

Wu, Zhang, Yao, Li, Han, Lian, Zhao and Nan (2016). "Cucurbitacin E ameliorates hepatic fibrosis in vivo and in vitro through activation of AMPK and blocking mTOR-dependent signaling pathway." Toxicol Lett 258: 147-158.

Wymore, Hempel, Cho, Mackerell, Nicholas and Deerfield (2004). "Molecular recognition of aldehydes by aldehyde dehydrogenase and mechanism of nucleophile activation." Proteins 57(4): 758-771.

Xie, Hou, Song, Yu, Huang, Sun, Kang and Tang (2016). "Ferroptosis: process and function." Cell Death Differ 23(3): 369-379.

Yagoda, von Rechenberg, Zaganjor, Bauer, Yang, Fridman, Wolpaw, Smukste, Peltier, Boniface, Smith, Lessnick, Sahasrabudhe and Stockwell (2007). "RAS-RAF-MEK-dependent oxidative cell death involving voltage-dependent anion channels." Nature 447(7146): 864-868.

Yang, Kim, Gaschler, Patel, Shchepinov and Stockwell (2016). "Peroxidation of polyunsaturated fatty acids by lipoxygenases drives ferroptosis." Proc Natl Acad Sci U S A 113(34): E4966-4975.

Yang, Liu, Li, Wu, Wang, You, Li, Ding, Liu and Gong (2018). "Predictive and preventive significance of AMPK activation on hepatocarcinogenesis in patients with liver cirrhosis." Cell Death Dis 9(3): 264.

Yang, Shimada, Delva, Patel, Ode, Skouta and Stockwell (2012). "Identification of Simple Compounds with Microtubule-Binding Activity That Inhibit Cancer Cell Growth with High

Potency." ACS Med Chem Lett 3(1): 35-38.

Yang, SriRamaratnam, Welsch, Shimada, Skouta, Viswanathan, Cheah, Clemons, Shamji, Clish, Brown, Girotti, Cornish, Schreiber and Stockwell (2014). "Regulation of ferroptotic cancer cell death by GPX4." Cell 156(1-2): 317-331.

Yang and Stockwell (2008). "Synthetic lethal screening identifies compounds activating iron-dependent, nonapoptotic cell death in oncogenic-RAS-harboring cancer cells." Chem Biol 15(3): 234-245.

Yu, Guo, Xie, Wang and Chen (2017). "Ferroptosis, a new form of cell death, and its relationships with tumourous diseases." J Cell Mol Med 21(4): 648-657.

Yuan, Gong, Luo, Zheng, Song, Ma, Guo, Hu, Thiel, Vinson, Hu, Wang and Li (2009). "Opposing roles for ATF2 and c-Fos in c-Jun-mediated neuronal apoptosis." Mol Cell Biol 29(9): 2431-2442.

Zhang (2009). "Non-Smad pathways in TGF-beta signaling." Cell Res 19(1): 128-139.

Zhang, Du, Qiao, Zhang, Zheng, Wu, Chen, Zhu, Liu, Bian, Guo, Yang, Ma, Yu, Pan, Sun and Wang (2019). "Ferroptosis is governed by differential regulation of transcription in liver cancer." Redox Biol 24: 101211.

Zhang, Shi, Liu, Feng, Gong, Koppula, Sirohi, Li, Wei, Lee, Zhuang, Chen, Xiao, Hung, Chen, Huang, Li and Gan (2018). "BAP1 links metabolic regulation of ferroptosis to tumour

suppression." Nat Cell Biol 20(10): 1181-1192.

Zhang, Zhang, Xie, Gao, Ma, Yuan, Li, Wang, Li, Zhang and Chu (2013). "Multitargeted inhibition of hepatic fibrosis in chronic iron-overloaded mice by Salvia miltiorrhiza." J Ethnopharmacol 148(2): 671-681.